

# The Electroweak Sector of the pMSSM in the Light of LHC - 8 TeV and Other Data

Manimala Chakraborti<sup>a1</sup>, Utpal Chattopadhyay<sup>a2</sup>, Arghya Choudhury<sup>b3</sup>, Amitava Datta<sup>c4</sup>, Sujoy Poddar<sup>d5</sup>

<sup>a</sup> Department of Theoretical Physics, Indian Association for the Cultivation of Science,  
2A & B Raja S.C. Mullick Road, Jadavpur, Kolkata 700 032, India

<sup>b</sup> Department of Physical Sciences, Indian Institute of Science Education and  
Research (IISER) - Kolkata, Mohanpur, Nadia, West Bengal - 741252, India

<sup>c</sup> Department of Physics, University of Calcutta, 92 A.P.C. Road, Kolkata 700 009, India

<sup>d</sup> Department of Physics, Netaji Nagar Day College, 170/436, N.S.C. Bose Road,  
Kolkata - 700092, India

## Abstract

Using the chargino-neutralino and slepton search results from the LHC in conjunction with the WMAP/PLANCK and  $(g - 2)_\mu$  data, we constrain several generic pMSSM models with decoupled strongly interacting sparticles, heavier Higgs bosons and characterized by different hierarchies among the EW sparticles. We find that some of them are already under pressure and this number increases if bounds from direct detection experiments like LUX are taken into account, keeping in mind the associated uncertainties. The XENON1T experiment is likely to scrutinize the remaining models closely. Analysing models with heavy squarks, a light gluino along with widely different EW sectors, we show that the limits on  $m_{\tilde{g}}$  are not likely to be below 1.1 TeV, if a multichannel analysis of the LHC data is performed. Using this light gluino scenario we further illustrate that in future LHC experiments the models with different EW sectors can be distinguished from each other by the relative sizes of the  $n$ -leptons +  $m$ -jets +  $\cancel{E}_T$  signals for different choices of  $n$ .

---

<sup>1</sup>tpmc@iacs.res.in

<sup>2</sup>tpuc@iacs.res.in

<sup>3</sup>arghyac@iiserkol.ac.in

<sup>4</sup>adatta@iiserkol.ac.in

<sup>5</sup>sujoy.phy@gmail.com

---

## Contents

<b>1</b>	<b>Introduction</b>	<b>2</b>
<b>2</b>	<b>The Constraints from <math>(g - 2)_\mu</math>, DM Relic Density and Other Experiments</b>	<b>7</b>
2.1	Higgs at 125 GeV . . . . .	7
2.2	Anomalous Magnetic Moment of Muon . . . . .	8
2.3	Dark Matter Relic Density and Results from Direct and Indirect Searches . . . . .	10
<b>3</b>	<b>Electroweak Sector of pMSSM Models in the Light of LHC and Other Constraints</b>	<b>12</b>
3.1	Light Gaugino and Left Slepton (LGLS) Scenario . . . . .	13
3.1.1	Tilted LGLS Scenario . . . . .	17
3.2	Light Gaugino and Light Left and Right Slepton (LGLRS) Scenario . . . . .	20
3.2.1	Tilted LGLRS Scenario . . . . .	22
3.3	Light Gaugino and Right Slepton (LGRS) Scenario . . . . .	25
3.4	Light Gaugino and Heavy Slepton (LGHS) Scenario . . . . .	26
3.5	Light Left Slepton (LLS) Scenario . . . . .	27
3.6	Light Left and Right Slepton (LLRS) Scenario . . . . .	28
<b>4</b>	<b>Direct and Indirect Detections of Dark Matter</b>	<b>30</b>
4.1	Direct Detection . . . . .	30
4.2	Indirect Detection of DM through Photon Signal . . . . .	32
<b>5</b>	<b>Gluino Mass Limits in Different Models and Their Characteristic Signatures</b>	<b>34</b>
<b>6</b>	<b>Conclusion</b>	<b>40</b>

---

## 1 Introduction

The LHC experiments at  $\sqrt{s} = 7/8$  TeV have concluded recently. The painstaking searches for supersymmetry (SUSY) [1–3], the most popular and attractive extension of the standard model

(SM) of particle physics have not observed any signal yet. Consequently stringent limits on the masses of the supersymmetric particles (sparticles) belonging to the strongly interacting sector, expected to be produced with large cross-sections, have been obtained by both the ATLAS and the CMS collaborations [4–8]<sup>1</sup>. Whether these limits already put question marks on the naturalness [10, 11] of various SUSY models may be debated in spite of the fact that it is hard to quantify the degree of naturalness. Naturalness or the absence of it should therefore be left at the stage of a healthy theoretical debate and not be regarded as the concluding remark on SUSY.

The minimal supersymmetric standard model (MSSM) [2, 3] has another important component - the electroweak (EW) sector. The production cross-sections of the sparticles belonging to this sector at the LHC are rather modest. As a result there was no constraint on the properties of these sparticles until recently. Thus some weak mass limits from LEP [12] and Tevatron [13, 14] were the only available information on this sector. The purpose of this paper is to focus on this sector in the light of the direct constraints from LHC [15–17] as well as indirect constraints like the observed value of the anomalous magnetic moment of the muon from the Brookhaven  $(g - 2)_\mu$  experiment [18] and the relic density constraints for dark matter from WMAP [19] or PLANCK [20] experiments. Using the combined constraints we then identify the allowed parameter space (APS).

We will also consider the constraints from direct [21–23] and a few selected indirect searches [24] of dark matter which may involve considerable theoretical and astrophysical uncertainties (to be elaborated in a subsequent section). In view of this we present our results in such a way that the effect of each constraint may separately be seen. We also study the prospect of future LHC searches and the issue of distinguishing several EW scenarios having different dark matter (DM) annihilation/coannihilation mechanisms leading to correct relic density (we will often refer this as DM producing mechanisms).

Since the SUSY breaking mechanism leading to a given pattern of sparticle masses is unknown, in the most general MSSM the above two sectors are unrelated. Only in models with high scale physics inputs due to considering specific mechanisms of SUSY breaking like the minimal supergravity (mSUGRA) [25], the masses of the strong and the EW sparticles are correlated. As a result, the stringent bounds on the former sector translate into bounds on the masses of the latter some of which are apparently much stronger than the direct limits. However, since the mechanism of

---

<sup>1</sup>However, these stringent bounds are reduced significantly in compressed SUSY type scenarios [9].

SUSY breaking is essentially unknown it is preferable to free ourselves from such model dependent restrictions.

Apart from particle physics, the EW sparticles may play important roles in cosmology as well. An attractive feature of all models of SUSY with R-parity [3] conservation is that the lightest supersymmetric particle (LSP) is stable. In many models the lightest neutralino  $\tilde{\chi}_1^0$  happens to be LSP. This weakly interacting massive particle is a popular candidate for the observed dark matter (DM) in the universe [26–28]. Moreover, the DM annihilation/coannihilation mechanisms leading to acceptable relic density for DM may be driven entirely by the electroweak sparticles [26, 28, 29]. Consequently the observed value of the DM relic density [19, 20] may effectively be used to constrain the EW sector or a specific SUSY model in particular.

It was recently emphasized in Ref. [30] that the physics of DM and the stringent LHC bounds on the squark and gluino masses, obtained mainly from the jets + missing energy data, are controlled by two entirely different sectors of the phenomenological MSSM (pMSSM) [31]. While the DM producing mechanisms may broadly be insensitive to the strong sector<sup>2</sup> of the pMSSM [31], the response of the above LHC bounds to changes in the EW sector parameters is rather weak. It was demonstrated by simulations at the generator level that these bounds change modestly for a variety of EW sectors with different characteristics all consistent with the DM relic density data [30]. Thus the strong constraints on DM production in mSUGRA [32, 33] due to squark-gluino mass bounds may be just an artifact of this model<sup>3</sup>.

It was further noted that in the unconstrained MSSM, there are many possible DM producing mechanisms which are not viable in mSUGRA due to the constraints on the squark-gluino masses. Some examples are LSP pair annihilation via Z or the lighter Higgs scalar (h) resonance, LSP-sneutrino coannihilation, coannihilation of a bino dominated LSP and a wino dominated chargino etc [30, 35]. It may be emphasized that the discovery of the Higgs boson by the LHC collaborations [36] has opened up the possibility of pinpointing the LSP pair annihilation via h-resonance.

Subsequently both the CMS and the ATLAS collaborations published direct search limits on the masses of the electroweak sparticles in several models sensitive to the LHC experiments at 7 TeV [37–39]. It was pointed out in Ref. [40] the models constrained by the LHC experiments are

---

<sup>2</sup>Except in situations like LSP-stop coannihilations.

<sup>3</sup>For a recent review focussing on recent searches for dark-matter signatures at the LHC see Ref. [34].

important in the context of DM physics as well since many of these models contain light sleptons either of L or R-type. It was demonstrated that even the preliminary mass bounds based on  $13 \text{ fb}^{-1}$  8 TeV data [41, 42] are able to put non-trivial constraints on parameter space in regard to the neutralino relic density bounds. It was also pointed out that additionally if the gluinos are relatively light (just beyond the reach of the current LHC experiments) these models with the lightest neutralino as the LSP may lead to novel collider signatures. Especially in models with light sleptons the same sign dilepton (SSD) signal may indeed turn out to be stronger than the canonical jets + missing energy signal. Moreover, one is able to distinguish different relic density satisfying mechanisms by measuring the relative rates of the  $n$ -leptons +  $m$ -jets + missing energy events for different values of  $n$ .

More recently the LHC collaborations have published their analyses for EW sparticle searches based on  $20 \text{ fb}^{-1}$  data [15–17] which, as expected, yield stronger mass bounds. The results were interpreted in terms of several simplified models. In this approach only the masses of a limited number of sparticles relevant to a particular signal are treated as free parameters, while the others are assumed to be decoupled. Moreover, in many cases the LSP is assumed to be bino dominated while the lighter chargino ( $\tilde{\chi}_1^\pm$ ) to be wino dominated, but all the parameters that determine the masses and the mixings in the EW gaugino sectors are not precisely identified. However, many of the above parameters which are moderately or marginally important for collider analyses, are quite important for computation of the indirect observables such as the observed DM relic density bounds or  $(g-2)_\mu$ . In view of this we have computed the bounds by a PYTHIA [43] based generator level analysis. We use the full set of pMSSM parameters sufficient to determine all relevant observables. We also obtain bounds in related models not considered by the LHC collaborations in Refs. [15–17].

We next consider a few indirect constraints in order of the level of stringency. We note that stringency of a constraint is increased if there is less model dependence while it is decreased if there is a large combined theoretical and experimental errors where some of the theoretical errors may not always even be precisely quantifiable. With the details mentioned in Sec. 2, the outline of the above constraints in the aforesaid order are given below: i) the precise dark matter relic density constraint from WMAP/PLANCK [19, 20] within the ambit of standard model of cosmology [44], ii) the  $(g-2)_\mu$  data that deviates from the SM result by more than  $3\sigma$  [18, 45, 46], (which is becoming more and more potent with the gradual reduction of the disagreement between the  $e^+e^-$

data based analyses and the ones that use hadronic  $\tau$ -decay data for evaluating the contributions for the hadronic vacuum polarisation part of the contributions to the theoretical estimation of  $(g-2)_\mu$  [47]), iii) the bound on the spin-independent direct detection cross-section of DM ( $\sigma_{\tilde{\chi}p}^{\text{SI}}$ ) from XENON100 [21] and LUX [22]. We also consider the reach of XENON1T [23] and iv) the indirect detection constraint from photon signal as given by the FERMI data [24]. With a bino-dominated LSP the last constraint is hardly of any interest as we will see in Sec. 4.

In the optimistic scenario of SUSY discovery in the LHC-13 TeV runs, it would still be difficult to pinpoint the underlying DM producing mechanism by explicitly reconstructing the sparticle spectrum. This is especially true for the early phase of the experiment. In this work we address the possibility of distinguishing various pMSSM scenarios, with characteristic EW sectors constrained by the experiments discussed above. This may be possible if at least one of the strongly interacting sparticles is within the reach of the LHC and its decays bear the imprints of the underlying EW sector as we will show in a later section.

In our analysis we will particularly see the effects of variations of  $\tan\beta$ , the ratio of the vacuum expectation values of the two neutral Higgs bosons,  $\mu$ , the higgsino mass parameter, the slepton masses etc. This will be explored in a generic scenario with bino dominated LSP and wino dominated  $\tilde{\chi}_1^\pm$  along with heavy squarks, gluino as well as large masses for the charged Higgs  $H^\pm$ , the heavier CP-even neutral Higgs  $H$  and the pseudoscalar Higgs  $A$  ( $M_{H^\pm}, M_H, M_A$  respectively). We will also consider a large top-trilinear parameter  $A_t$  so that the lighter Higgs mass  $m_h$  agrees with the observed value in the least possible mass reach of the super-partners.

The plan of this paper is as follows. In Sec. 2 we will review the effect of Higgs mass data as applied to pMSSM and indirect constraints like that from  $(g-2)_\mu$ , WMAP/PLANCK data for relic density of DM and the effect of XENON100, LUX and the future XENON1T on our analysis. In Sec. 3 we will explore various electroweak sectors by having the left and right slepton masses (separately or together) in between the masses of the LSP and the lighter chargino. This will be analysed by considering sufficiently large values of  $\mu$  such that one always obtains a bino-dominated LSP and a wino-dominated  $\tilde{\chi}_1^\pm$ . We will find the APS from collider bounds and constraints from the relic density as well as  $(g-2)_\mu$ . In Sec. 4 we will further impose the constraints for spin-independent direct detection cross-section limits from LUX and  $\gamma$ -ray constraints for indirect detection of DM from Fermi-LAT. In Sec. 5 we will analyse a few benchmark points chosen from the models of Sec. 3

and discuss the prospects of distinguishing various models. We will conclude in Sec. 6.

## 2 The Constraints from $(g - 2)_\mu$ , DM Relic Density and Other Experiments

We work in a pMSSM framework where parameters are chosen such that the strongly interacting sector is beyond the reach of the LHC. We set all squark masses at 2 TeV. While probing the electroweak sector via the relevant constraints we remind ourselves that the mass eigenstates namely the charginos ( $\tilde{\chi}_i^\pm$ ,  $i = 1, 2$ ) and the neutralinos ( $\tilde{\chi}_i^0$ ,  $i = 1-4$ ) are composed of the  $SU(2)$  gauginos (the winos), the  $U(1)$  gaugino (the bino) and the higgsinos (the superpartners of the Higgs bosons) with appropriate charges. The degrees of mixing are essentially controlled by 4 free parameters - the gaugino mass parameters  $M_1$  and  $M_2$ , the higgsino mass parameter  $\mu$  and  $\tan\beta$ , the ratio of the vacuum expectation values of the two Higgs doublets. For  $|\mu| \gg |M_2| > |M_1|$ ,  $\tilde{\chi}_1^0$  is bino ( $\tilde{B}$ ) dominated and the lighter chargino  $\tilde{\chi}_1^\pm$  (the second lightest neutralino  $\tilde{\chi}_2^0$ ) is mostly a charged (neutral) wino, but for  $|M_1| > |M_2|$ ,  $\tilde{\chi}_1^0$  ( $\tilde{\chi}_2^0$ ) is dominantly the neutral wino (bino). On the other hand, if  $|M_1| \simeq |M_2|$  the two lighter neutralinos are admixtures of the neutral wino and bino. In the limit,  $|\mu| \ll |M_1|, |M_2|$ ,  $\tilde{\chi}_1^0$  and  $\tilde{\chi}_2^0$  and the lighter chargino  $\tilde{\chi}_1^\pm$  are all mostly higgsinos having approximately the mass  $|\mu|$ . A scenario with  $|\mu| \simeq |M_1| \simeq |M_2|$  would result into strong mixing for the concerned mass eigenstates. In this analysis we consider only bino-dominated LSP ( $\tilde{\chi}_1^0$ ) and wino-dominated  $\tilde{\chi}_1^\pm$ . The production cross-section of  $\tilde{\chi}_1^\pm$ ,  $\tilde{\chi}_2^0$  would be drastically reduced for a consideration of a higgsino dominated  $\tilde{\chi}_1^\pm$  which would in turn weaken the exclusion limits in the  $m_{\tilde{\chi}_1^0} - m_{\tilde{\chi}_1^\pm}$  plane.

We start our analysis by reviewing a few relevant constraints like the measured Higgs boson mass, gyromagnetic ratio of the muon and cold dark matter relic density.

### 2.1 Higgs at 125 GeV

We note that a study within MSSM should most importantly accommodate the lighter Higgs boson mass  $m_h$  to be at 125 GeV [36]. This has generally pushed up SUSY spectra to high masses in general for models like mSUGRA. However, the required large loop corrections to the Higgs boson mass primarily arise from loops involving top-squarks and these contributions can be controlled via

considering large trilinear coupling parameter  $A_t$  ( $\sim -2$  to  $-3$  TeV) leading to reduction of the average mass scale of the SUSY spectra [48]. We require the lighter Higgs scalar mass to be in the interval  $122 < m_h < 128$  GeV in MSSM. The spread is considered to accommodate a theoretical uncertainty of about 3 GeV in computing the Higgs mass. This indeed originates from uncertainties in the renormalisation scheme, scale dependence, the same in higher order loop corrections up to three loops or that due to the top-quark mass [49]. The other Higgs bosons are assumed to be decoupled.

Due to precise measurement of  $m_h$  at LHC experiments [36], it is now possible to explore the specific regions of parameter space where the LSP pair annihilation occurs via Higgs (h-resonance). We recall that this occurs for  $m_{\tilde{\chi}_1^0} \approx m_h/2$ . This enables us in examining critically the viability of this mechanism in different models, as we will show in the subsequent sections.

Limits on the masses of the charginos and the neutralinos from trilepton data crucially depend on the leptonic BR of these sparticle. When the decay mode  $\tilde{\chi}_2^0 \rightarrow h\tilde{\chi}_1^0$  is kinematically allowed, the mass limits become reduced significantly [50]. The information on the Higgs mass enables one in assessing the impact of this ‘spoiler mode’<sup>4</sup> on the trilepton data in a more precise way. In a subsequent section we shall take up the issue once more.

## 2.2 Anomalous Magnetic Moment of Muon

The Muon Anomalous Magnetic Moment ( $a_\mu = \frac{1}{2}(g-2)_\mu$ ) is an important probe for the signatures of new physics [52]. A generic contribution to  $a_\mu$  scales like  $m_\mu^2/\Lambda^2$  where  $\Lambda$  and  $m_\mu$  refer to the scale of new physics and muon mass respectively. The experimental data of  $a_\mu$  namely  $a_\mu^{\text{exp}}$  [18] differs significantly from the Standard Model evaluation  $a_\mu^{\text{SM}}$  [45, 46]. Thus  $\Delta a_\mu = a_\mu^{\text{exp}} - a_\mu^{\text{SM}}$  can be an effective probe for a beyond the standard model (BSM) physics provided  $\Lambda$  is not too large.  $a_\mu^{\text{SM}}$  may be broken into a part coming from pure quantum electrodynamics, a part coming from hadronic contributions and finally a part from Electroweak physics involving vector bosons and Higgs boson [52]. We note that the level of disagreement of  $a_\mu^{\text{exp}}$  from the SM result is of the same order as the contributions from electroweak corrections [45, 46].  $a_\mu^{\text{SM}}$  itself has a significant amount of error primarily because of the uncertainties arising out of the hadronic vacuum polarization and the light-by-light scattering contributions [45, 46, 52]. We note that the hadronic vacuum

---

<sup>4</sup>A few recent analyses in this context may be seen in Refs. [51].



polarization part has two different evaluations based on i)  $e^+e^-$  and ii) hadronic  $\tau$ -decay data [52]. The difference of the two evaluations which has been diminishing over the years still affects  $\Delta a_\mu$  to an appreciable degree [47]. The resulting discrepancy that amounts to more than  $3\sigma$  level of deviation is summarized as follows [46].

$$\Delta a_\mu = a_\mu^{\text{exp}} - a_\mu^{\text{SM}} = (29.3 \pm 9.0) \times 10^{-10}. \quad (1)$$

The contributions of different parts of  $a_\mu^{\text{SM}}$  may be seen in Ref. [46]<sup>5</sup>.

The supersymmetric contribution to  $a_\mu$  namely  $a_\mu^{\text{SUSY}}$  may be as large as the electroweak contribution for parts of parameter space associated with lighter electroweak sector super-partners like charginos, sneutrinos, neutralinos or smuons as well as for large  $\tan\beta$  [53]. It may, therefore, potentially explain the discrepancy  $\Delta a_\mu$  of Eq.1. Alternatively, SUSY parameter space can effectively be constrained with a given set of lower and upper bounds of  $\Delta a_\mu$ . Thus the limits of  $a_\mu^{\text{SUSY}}$  at the level of  $2\sigma$  and  $3\sigma$  are as follows.

$$11.3 < a_\mu^{\text{SUSY}} \times 10^{10} < 47.3 \quad (2\sigma) \quad \text{and} \quad 2.3 < a_\mu^{\text{SUSY}} \times 10^{10} < 56.3 \quad (3\sigma). \quad (2)$$

Details of  $a_\mu^{\text{SUSY}}$  in the MSSM based scenarios including mSUGRA and various models with high scale physics input were studied several years ago for which a partial list may be seen in Refs. [53–56]. At one-loop level,  $a_\mu^{\text{SUSY}}$  arises from loops containing chargino and sneutrino ( $\tilde{\chi}_i^\pm - \tilde{\nu}_\mu$ ) and the same containing neutralino and smuon ( $\tilde{\chi}_i^0 - \tilde{\mu}_j$ ).  $a_\mu^{\text{SUSY}}$  increases with  $\frac{1}{\cos\beta} \sim \tan\beta$  and in general for models like mSUGRA with universal boundary conditions the chargino loop containing the lighter chargino state is the most dominating one [54]. This dominance results into a correlation of the sign of  $\mu M_2$  with that of  $a_\mu^{\text{SUSY}}$  [54], in models like mSUGRA. This is however not true in the general scenario of MSSM in spite of the fact that the lighter chargino loop ( $\tilde{\chi}_1^\pm - \tilde{\nu}_\mu$ ) still dominates over the other contributions for a large zone of parameter space [55]. The neutralino loop contributions can be significantly large for smaller smuon masses and for cases with large  $|\mu M_1|$  [56]. For the cases where neutralino loop contribution dominates the signs of  $a_\mu^{\text{SUSY}}$  and  $M_1\mu$  become the same<sup>6</sup>. In this work, the signs of  $M_1$ ,  $M_2$  and that of  $\mu$  are considered positive.

---

<sup>5</sup>Considering all the uncertainties of  $a_\mu^{\text{SM}}$  including those arising from light-by-light scattering contributions there are analyses which estimate a much larger error going almost up to  $5\sigma$  (see the comments in Ref. [46]).

<sup>6</sup>We note that  $a_\mu^{\text{SUSY}}$  can be large for a large left-right smuon mixing [57].

In this analysis we will mostly focus on the pMSSM parameter space which is consistent with the  $\Delta a_\mu$  constraint upto the level of  $2\sigma$  following Eq.2. Of course compared to a  $2\sigma$  level, requiring a consistency at the level  $3\sigma$  would be highly conservative but we have occasionally taken recourse to it. Henceforth we will require the APS to satisfy this level of consistency.

An important point to note is that a large range of  $a_\mu^{\text{SUSY}}$  may put strong upper bounds on the super-partner masses in addition to indicating definite lower bounds for the same [58]. Particularly with the announcement of Higgs boson discovery, and/or with the latest LHC data of squark and gluino masses, models having limited number of high scale physics inputs such as mSUGRA can hardly accommodate the above constraint [59]. However, non-universal SUGRA models can still accommodate the above non-vanishing  $\Delta a_\mu$  apart from generic MSSM models with a larger set of inputs [60] .

### 2.3 Dark Matter Relic Density and Results from Direct and Indirect Searches

We will now come to the discussion of possible mechanisms of satisfying the observed relic density from WMAP and PLANCK data in our analysis. Similar to the limits used in Ref. [61] we consider a  $2\sigma$  level of WMAP nine year data [19]<sup>7</sup> bound with a 10% error in theoretical estimation as follows. This range also embraces the  $3\sigma$  limits from PLANCK [20].

$$0.092 < \Omega_{\tilde{\chi}} h^2 < 0.138. \quad (3)$$

Here, we will select only the lightest neutralino as the cold dark matter candidate. The LSP is sufficiently bino-dominated. Hence in general the possible annihilation mechanisms would be exchange of sleptons in the  $t$ -channel (bulk annihilation), LSP-annihilation via  $s$ -channel Higgs pole or even via Z-pole. The LSP can undergo coannihilation with a scalar particle like the stau or the sneutrino, since top-squarks are assumed to be very heavy. However, considering the present bounds of sparticle masses mSUGRA is not able to accommodate many of the above annihilation/coannihilation scenarios because of its associated correlations among sparticle masses as well as due to constraints like Higgs mass. For example, a neutralino with mass  $= M_Z/2$  is ruled out by LEP bound on chargino mass when the gaugino mass unification condition is applied. We will identify the actual mechanisms in the parameter space of each model that would survive the combined analysis of

---

<sup>7</sup>We consider the eCMB+BAO+ $H_O$  value of Table 4 of Ref. [19].

LHC, CDM and precision data like  $(g - 2)_\mu$ .

In addition to the constraint from dark matter relic density, we will also investigate the possibility of direct detection of dark matter via computing spin-independent LSP-proton scattering cross-section  $\sigma_{\tilde{\chi}p}^{\text{SI}}$  in relation to the XENON100 [21] and LUX [22] data.  $\sigma_{\tilde{\chi}p}^{\text{SI}}$  results from diagrams involving  $t$ -channel Higgs and  $s$ -channel squark exchanges. Unless the squark masses are close to the mass of the LSP which is certainly not our case after the LHC data, the Higgs exchange diagrams contribute dominantly to the above cross-section [62]. The effective couplings are dependent on the nature of composition of the LSP. Since the  $h(H) - \tilde{\chi}_1^0 - \tilde{\chi}_1^0$  couplings involves product of gaugino and higgsino components of the neutralino diagonalising matrix, only for the presence of a sufficient higgsino within  $\tilde{\chi}_1^0$  the direct detection cross-section  $\sigma_{\tilde{\chi}p}^{\text{SI}}$  may become appreciable [63].

We should however keep in mind various uncertainties in computing the cross-section  $\sigma_{\tilde{\chi}p}^{\text{SI}}$  arising from particle physics or astrophysics related issues<sup>8</sup>. There is a significant amount hadronic uncertainty in evaluating  $\sigma_{\tilde{\chi}p}^{\text{SI}}$ . The strangeness content of nucleon is quite important for evaluating the cross-section. This is because, for WIMP-nucleon scattering the WIMP couplings with valence quarks like  $u$  and  $d$ -quarks are small due to small Yukawa couplings. Thus the contributions to scattering amplitude due to heavy sea quarks become important (light quarks as sea quarks again have small contribution to the amplitude). Over the last few years the strangeness contribution to proton mass is effectively reduced via lattice computations [65]. This in turn may potentially reduce the uncertainties in the evaluation of effective couplings of LSP-nucleon interactions leading to more precise results. We compute all the dark matter related quantities using micrOMEGAs (version-3.2) [66]. Unlike the previous versions, micrOMEGAs (version-3.2) treated the above error by using a different prescription for evaluating the strange quark content of a nucleon. A weighted average of  $\sigma_s = m_s < p|\bar{s}s|p >$ , a measure of strangeness content was obtained out of various lattice quantum chromodynamics (QCD) results. We must note that although we have used the default values of  $\sigma_s$  as obtained by the weighted average as mentioned above, the individual lattice results used in this averaging vary widely from each other<sup>9</sup> leading to enough uncertainty in the direct detection cross-section. Additionally, we should also keep in mind the uncertainties of

---

<sup>8</sup>Apart from particle physics and astrophysics related uncertainties, see also Ref. [64] for the uncertainty arising out of poor knowledge of cosmic ray activation in detector materials in regard to direct detection backgrounds.

<sup>9</sup>See Table 1 of Ref. [66]

astrophysical origin in finding the rate of dark matter events in a given detector. Among the above, uncertainties may arise from determination of the local dark matter density [67,68]. Consideration of the existence of non-Maxwellian velocity distributions for WIMP also shows an adequate amount of variation in the direct detection rates [69,70] specially for low mass DM. Apart from the current data we will also relate our result with the reach of the future experiment XENON1T [23] that would be about two orders of magnitude below the current LUX [22] or XENON100 [21] limit for the scalar cross-section and can probe various SUSY models even if the above uncertainties continues to persist.

Besides the direct detection limits we would also explore the reach of indirect detection data from Fermi-LAT [24] for continuous  $\gamma$ -ray signal from dense astrophysical regions such as galactic center, dwarf galaxies etc. With a highly bino-dominated LSP, expectedly, our scenarios produce too little cross-section ( $< \sigma v >$ ).

In the next section we intend to describe various models that are based on different relative masses of the EW sparticles. We will analyse these models particularly for interesting collider signatures while also imposing the necessity to satisfy the Higgs mass, the  $(g-2)_\mu$  and the cold dark matter constraints and of course the LEP limits on chargino and slepton masses [12]. Only after filtering out the APS we will explore the degree of constraints from the XENON100 and the LUX data keeping in mind the extent of theoretical and astrophysical uncertainties in the direct detection of dark matter which could at least be an order of magnitude or even more.

### 3 Electroweak Sector of pMSSM Models in the Light of LHC and Other Constraints

The non-observation of the charginos, neutralinos as well as the sleptons at the LHC severely constrains several pMSSM models sensitive to the LHC searches. They are particularly important in the era of a known mass of the Higgs boson. We will focus on bino-dominated  $\tilde{\chi}_1^0$  and wino-dominated  $\tilde{\chi}_1^\pm/\tilde{\chi}_2^0$  which are very sensitive to the LHC searches. This scenario can be easily realized by considering a large  $\mu$  and adjusting the gaugino mass parameters of the electroweak sector. We will analyse various scenarios of left and right slepton mass parameters ( $M_{\tilde{l}_L}, M_{\tilde{l}_R}$ ) placed differently with respect to the electroweak gaugino mass parameters  $M_1$  and  $M_2$ . The specific

choices are motivated by the direct production limits on electroweak sparticle masses by ATLAS and CMS [15–17] and the other observables under consideration. Each scenario may have important signatures in regard to collider physics, dark matter relic density and precision observables like  $(g - 2)_\mu$ . Our task is to find the APS after imposing the combined constraints and assess the possibility of observing EW SUSY particles in future LHC experiment.

For the detailed study we choose the following pMSSM parameters. All squark mass parameters as well as  $M_3$  and  $M_A$ , which hardly affect the observables under consideration, are set to a large value of 2 TeV. A choice of the trilinear coupling  $-3 \text{ TeV} < A_t < -2 \text{ TeV}$  is made for consistency with the measured mass of the lighter Higgs boson without the need of a very large sparticle mass scale. All other trilinear couplings are vanishing namely  $A_b = A_\tau = A_u = A_d = A_e = 0$ .  $M_1$ ,  $M_2$ ,  $\mu$ ,  $M_{\tilde{l}_L}$  and  $M_{\tilde{l}_R}$  are varied in this study where the relevant SM parameters considered are  $m_t^{\text{pole}} = 173.2 \text{ GeV}$ ,  $m_b^{\overline{MS}} = 4.19 \text{ GeV}$  and  $m_\tau = 1.77 \text{ GeV}$ .

### 3.1 Light Gaugino and Left Slepton (LGLS) Scenario

In this model it is assumed that only left sleptons are lighter than  $\tilde{\chi}_1^\pm$  and  $\tilde{\chi}_2^0$  while right sleptons are heavy. The ATLAS collaboration have searched for chargino-neutralino ( $\tilde{\chi}_1^\pm - \tilde{\chi}_2^0$ ) pair production leading to the trilepton signal for  $20 \text{ fb}^{-1}$  [15] of data. The results were interpreted in this simplified model. Here the L-sleptons ( $\tilde{l}_L$ ) of all the generations have masses midway between the masses of  $\tilde{\chi}_1^\pm$  and  $\tilde{\chi}_1^0$  whereas the R-sleptons ( $\tilde{l}_R$ ) are chosen to be very heavy leading to very small mixing effects in the slepton mass matrices. The sneutrinos are assumed to be degenerate with  $\tilde{l}_L$ , i.e.,  $M_{\tilde{l}_L} = M_{\tilde{\nu}} = (m_{\tilde{\chi}_1^0} + m_{\tilde{\chi}_1^\pm})/2$ . It was further assumed that the lightest neutralino is highly bino dominated and  $\tilde{\chi}_1^\pm$  or  $\tilde{\chi}_2^0$  are wino dominated. As a result the branching ratio (BR) of chargino decay into slepton-neutrino and sneutrino-lepton modes of each flavour is the same. Similarly  $\tilde{\chi}_2^0$  would decay into neutrino-sneutrino and lepton-slepton pairs of each flavour with equal probability. The non-observation of signal yielded the exclusion contour in Fig.8a of Ref. [15] which is reproduced in Fig.1(a) (see the black contour) for ready reference.

In order to validate our simulation we compute the above exclusion contour using PYTHIA (v6.428) [43]. The next to leading order (NLO) cross-section for the  $\tilde{\chi}_1^\pm \tilde{\chi}_2^0$  pair production have been computed by PROSPINO 2.1 [71] with CTEQ6.6M PDF [72]. Our simulation is based on those selection criteria of the ATLAS collaboration which may be implemented at the generator

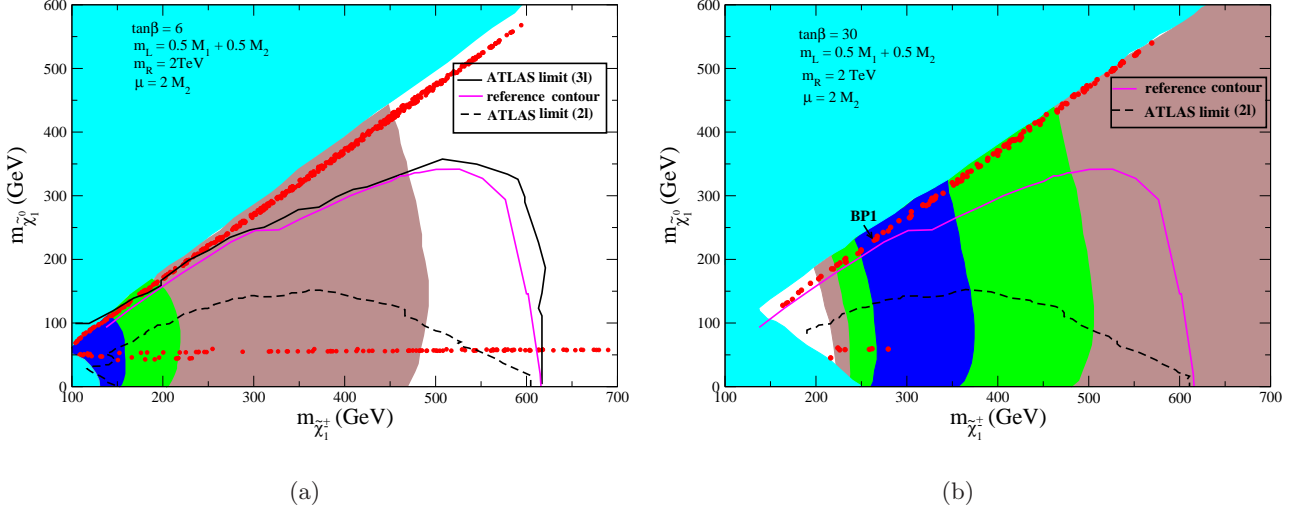


Figure 1: Plot in the  $m_{\tilde{\chi}_1^\pm} - m_{\tilde{\chi}_1^0}$  plane for the LGLS scenario with the slepton mass parameter satisfying  $M_{\tilde{L}} = 0.5M_1 + 0.5M_2$  for  $\tan\beta = 6$  (a) and 30 (b).  $M_{\tilde{L}}$  is chosen to be at 2 TeV. Here,  $m_{L/R} \equiv M_{\tilde{L}/R}$ . The blue, green and brown regions represent the parameter space where  $a_\mu^{\text{SUSY}}$  is consistent with  $\Delta a_\mu$  upto the level of  $1\sigma$ ,  $2\sigma$  and  $3\sigma$  respectively. The red points in the plot satisfy the relic density constraint from WMAP/PLANCK data. The parameters used for computing these and other observables are shown on the upper left corner of each figure. The cyan region corresponds to the parameter space which is discarded by theoretical constraints and the LEP limits on the slepton mass [12]. The black line in the left plot (a) represents the exclusion contour at 95% CL obtained by the ATLAS collaboration at 8 TeV LHC from trilepton searches [15]. The magenta line (the reference contour) shows the exclusion limit obtained by our simulation. The dashed line refers to the boundary of the disallowed region corresponding to the slepton search limits from 8 TeV ATLAS data [16] (see Fig.9). For the case of  $\tan\beta = 30$  (b), only the reference contour resulting from our simulation is shown. Throughout this paper we shall follow the same colour coding and conventions as used in this figure.

level. These are divided into several signal regions (SRs) : SRnoZa, SRnoZb and SRnoZc (see Table 1 of Ref. [15]). Each SR is characterized by a set of kinematical cuts and an upper bound on the effective cross-section ( $\sigma_e \equiv \text{production cross-section} \times \text{efficiency} \times \text{acceptance}$  or equivalently on  $N_{BSM}$  (number of events from BSM physics) obtained from the observed number of events and the SM background. These constraints are also expressed in terms of  $N_{BSM}$ , the maximum allowed number of beyond standard model events. Any model point is excluded if its associated  $\sigma_e$  exceeds

the above upper bound for at least one of the above SRs. Although we have not included the detector effects directly, we have introduced an approximate prescription for the combined trigger and electron (muon) identification efficiencies for different values of the transverse momentum ( $P_T$ ) following an analysis of ATLAS collaboration [73]. We confirm that the above prescription reproduces the efficiencies mentioned in the Table 5 of Ref. [15]. The above efficiency is chosen to be 75% (90%) for electrons with  $10 < P_T < 30$  ( $P_T > 30$ ). The same is chosen to be 85% for muons with  $P_T > 10$ . We have implemented electron/muon - jet isolation according to the ATLAS prescription [15].

Our exclusion contour, namely the magenta curve in Fig.1(a), for  $\tan\beta = 6$  validates the simulation. Henceforth this will be called the *reference contour*. Our representative choice of a few other SUSY parameters essential for computing the observables discussed in Sec. 2 are given in the upper left corner. We emphasize that the LHC exclusion contours are in general fairly insensitive to such choices. Additionally, we note that there is a less than 10 percent disagreement between the two results for  $m_{\tilde{\chi}_1^\pm} > 500$  GeV. We will come back to this issue soon. We note that  $m_{\tilde{\chi}_1^\pm} > 500$  GeV is disfavoured, in any case, either by the  $(g-2)_\mu$  or LHC data or by both. Henceforth, we will paste this reference contour in all the figures up to Fig.6 for comparison with other models.

The following minor differences with the ATLAS paper may be noted. For simplicity of computation we have scanned  $M_1$  and  $M_2$  while keeping L-slepton mass parameter midway, i.e.,  $M_{\tilde{l}_L} = \frac{1}{2}(M_1 + M_2)$ , instead of equating the physical slepton mass with  $\frac{1}{2}(m_{\tilde{\chi}_1^0} + m_{\tilde{\chi}_1^\pm})$ . With a highly bino-dominated  $\tilde{\chi}_1^0$  and wino-dominated  $\tilde{\chi}_1^\pm$ , the above approximation would be good upto a few percent level. Additionally, unlike what was used by ATLAS we do not assume any sneutrino-slepton mass degeneracy and entirely rely on the MSSM specified mass relations involving the D-term throughout our analysis. This increases the branching ratio of the decay  $\tilde{\chi}_2^0 \rightarrow \tilde{\nu}\bar{\nu}$  by a small but non-negligible amount and reduces the trilepton signal resulting in a weaker limit. Had we carried out our simulation following exactly the same assumptions as ATLAS our limits on  $m_{\tilde{\chi}_1^0}$  for  $m_{\tilde{\chi}_1^\pm} > 500$  GeV would have been even closer to that obtained by ATLAS. Furthermore, we have shown the effect of the direct slepton search limit from the 8 TeV ATLAS data [16]<sup>10</sup> by the black dashed line. The region within this contour is disfavoured. We denote the physical masses of left and right sleptons of first two generations by  $M_{\tilde{l}_{L/R}}^D$  taking into account the D-term contributions.

---

<sup>10</sup>see Fig.9

Similarly, for the sneutrinos we use the notation,  $M_{\tilde{\nu}}^D$ . We clearly see that no additional parameter space is discarded by the slepton search limit in the LGLS scenario other than what is already excluded by the trilepton data.

We now incorporate the theoretical and indirect constraints like  $(g-2)_\mu$  and the WMAP/PLANCK limits on dark matter relic density. In Fig.1(a) the upper cyan region corresponds to the parameter space which is discarded by the requirement of the LSP to be the lightest neutralino. The similarly coloured lower region is excluded via LEP limits on the slepton masses [12]. In the dark blue, green and light brown regions  $a_\mu^{\text{SUSY}}$  can explain the  $\Delta a_\mu$  anomaly (Eq.1) upto the level of  $1\sigma$ ,  $2\sigma$  and  $3\sigma$  respectively. Both lower and upper limits on  $a_\mu^{\text{SUSY}}$  have been considered only for parameter regions satisfying theoretical/LEP constraints. With almost a proportional dependence of  $a_\mu^{\text{SUSY}}$  on  $\tan\beta$  the contribution of  $a_\mu^{\text{SUSY}}$  in Fig.1(a) is small because of small value of  $\tan\beta$ . We note that the right handed sleptons being heavy in all the LGLS scenarios,  $a_\mu^{\text{SUSY}}$  is dominantly contributed by the lighter chargino-sneutrino loop diagrams.

The WMAP/PLANCK allowed regions satisfying Eq.3 for the dark matter relic density are shown as red circles<sup>11</sup>. We note that the regions satisfying the dark matter relic density limits are separated into top and bottom limbs. The parameter points denoted by red circles in the lower limb satisfy the relic density limits by LSP annihilations via a  $s$ -channel light Higgs boson resonance of mass  $\approx 125$  GeV. Additionally, there are some points that are associated with LSP pair annihilating via a  $s$ -channel Z resonance. The upper red points satisfy the dark matter limits via coannihilation of LSP with a sneutrino or a slepton almost equally. Besides the above there can be coannihilations between sleptons and sneutrinos or even a lighter chargino and a sneutrino in this region. Furthermore, for low mass zones of the figure one finds some degree of bulk annihilations both for the upper and the lower limbs.

From the LHC data at 8 TeV all parameter space which agrees with  $\Delta a_\mu$  up to the  $2\sigma$  level is almost excluded leaving a tiny region consistent with the combined constraint. Moreover, LHC data exclude the Higgs resonance region for  $m_{\tilde{\chi}_1^\pm} < 620$  GeV. The part of the parameter space with larger  $m_{\tilde{\chi}_1^\pm}$ , however, is consistent with the  $\Delta a_\mu$  constraint only at the level of  $3\sigma$ .

Fig.1(b) shows the analysis for a larger value of  $\tan\beta$  ( $= 30$ ) while keeping the same combination of other mass parameters. The colour codings are the same as in Fig.1(a). The cyan shaded lower

---

<sup>11</sup>In all the figures in this paper we shall follow the same colour convention.



region is excluded via LEP limits on the slepton masses or sneutrinos becoming tachyonic due to its negatively contributing D-term part, where the latter increases with  $\tan\beta$  in magnitude. In the white region  $a_\mu^{\text{SUSY}}$  differs from  $\Delta a_\mu$  by more than  $3\sigma$  because in this region of smaller  $m_{\tilde{\chi}_1^\pm}$ ,  $a_\mu^{\text{SUSY}}$  attains a very large value.

The prospect of finding a larger APS improves since  $a_\mu^{\text{SUSY}}$  increases for large  $\tan\beta$ . On the other hand, an increased  $\tan\beta$  hardly has any effect on the LHC constraints. This is expected since the mixing effects in the stau mass matrix is not significant even for larger  $\tan\beta$ , a result of considering very heavy R-sleptons (2 TeV). Thus with lighter stau having similar mass with that of selectron the BRs of  $\tilde{\chi}_1^\pm$  and  $\tilde{\chi}_2^0$  for leptonic decays remain unaltered while going from Fig.1(a) to Fig.1(b). The same can be said about the upper limb of the WMAP/PLANCK allowed region.

Focusing on Fig.1(b) we find that for relatively small  $M_2$  or  $m_{\tilde{\chi}_1^\pm}$  LSP-pair annihilation via light Higgs boson resonance is possible for producing the right relic abundance but the parameter space is forbidden by the LHC data. On the other hand, for larger  $m_{\tilde{\chi}_1^\pm}$ , the above resonance annihilation is not sufficient to give rise to an acceptable relic abundance in Fig.1(b). Indeed, it disappears completely outside the LHC forbidden region. There are two reasons that are important to note in this context. First,  $h - \tilde{\chi}_1^0 - \tilde{\chi}_1^0$  coupling decreases with increasing  $\tan\beta$ . Second, our choice of  $\mu = 2M_2$  that ensures  $\tilde{\chi}_1^\pm$  to be wino-dominated, causes reduction of the higgsino content of the LSP with increase of  $M_2$ , which in turn results into reduced LSP pair annihilation via  $h$ -resonance leading to over-abundance of dark matter. For the rest of the analysis we will see that for a wino dominated  $\tilde{\chi}_1^\pm$  and bino dominated LSP, LSP-pair annihilation via the  $h$ -resonance is disfavoured in general for large values of  $\tan\beta$  for the above reasons.

### 3.1.1 Tilted LGLS Scenario

We now explore the situation where the L-slepton mass is shifted from the mean of the lighter chargino and the lightest neutralino masses. We conveniently introduce the shift as follows<sup>12</sup>

$$M_{\tilde{l}_L} = xM_1 + (1-x)M_2. \quad (4)$$

where the tilting parameter  $x$  (with  $0 < x < 1$ ) determines the degree of closeness of  $M_{\tilde{l}_L}$  and  $m_{\tilde{\chi}_1^0}$ . The LGLS scenario analysed by ATLAS corresponds to  $x = \frac{1}{2}$ .

---

<sup>12</sup> The physical slepton mass is obtained by adding the D-term to the RHS of Eq.4.

We will consider two cases i) LGLS- $\tilde{\chi}_1^0$ : here  $x = 0.75$ , indicating L-slepton masses to be closer to the mass of the LSP than that of  $\tilde{\chi}_1^\pm$  and ii) LGLS- $\tilde{\chi}_1^\pm$ : here  $x = 0.25$ , making L-slepton mass parameters to be closer to the mass of  $\tilde{\chi}_1^\pm$ .

We will see soon that such variants of LGLS scenarios would hardly affect  $a_\mu^{\text{SUSY}}$ , mildly change the relic density satisfying properties for dark matter, but significantly change the size of the trilepton signal. The latter leads to changed exclusion contours compared to the LGLS scenario considered by ATLAS. This in turn may change the APS consistent with all the constraints.

### i) LGLS- $\tilde{\chi}_1^0$ :

In the analysis leading to Fig.2(a), we consider  $x = 0.75$ , while all other relevant parameters are kept same as in Fig.1(a). The lower cyan region is excluded due to tachyonic sneutrinos, sneutrino becoming the LSP and the LEP limits on  $\tilde{\chi}_1^\pm$  masses. In regard to  $(g-2)_\mu$  the dominant SUSY diagrams contributing to  $a_\mu^{\text{SUSY}}$  are not different from those of Fig.1(a). As a result the  $(g-2)_\mu$  constraint is almost insensitive to the modest variation of  $M_{\tilde{L}_L}$ . Hence, the  $1\sigma$ ,  $2\sigma$ , and  $3\sigma$  allowed regions do not change appreciably with respect to Fig.1(a).

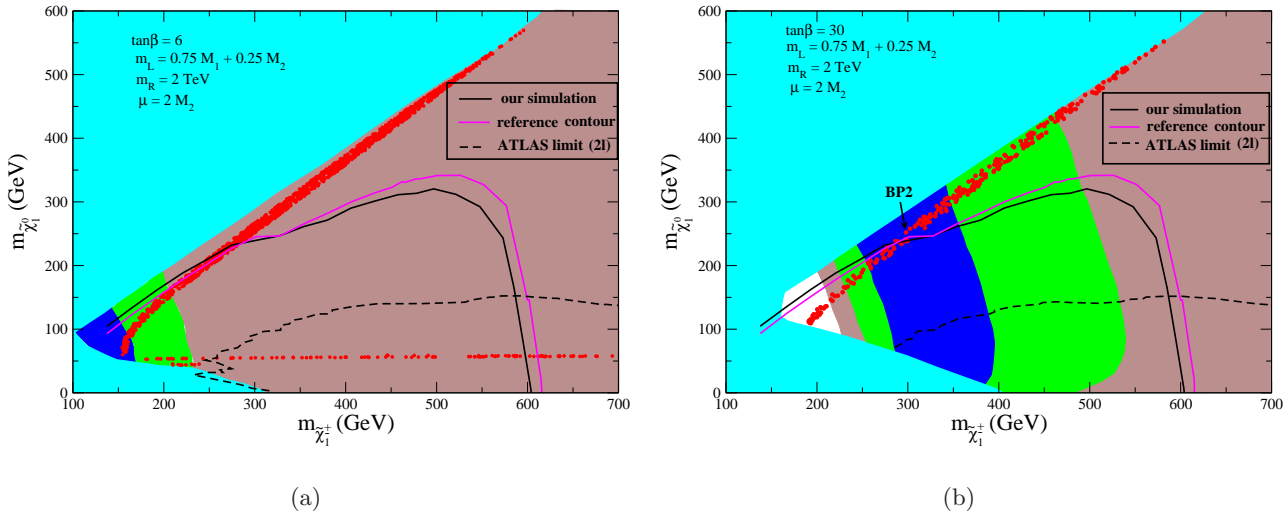


Figure 2: Plot in the  $m_{\tilde{\chi}_1^\pm} - m_{\tilde{\chi}_1^0}$  with the slepton mass parameter satisfying  $M_{\tilde{L}_L} = 0.75M_1 + 0.25M_2$  for  $\tan\beta = 6$  (a) and 30 (b). Colours and conventions are the same as in Fig.1. The exclusion contour for this scenario obtained by us is represented by the black line. The lower discarded region depending on the parameter point may be sensitive to the choice of the scale in the REWSB conditions.

Since the sleptons are closer in mass to that of  $\tilde{\chi}_1^0$ , the leptons arising from decays  $\tilde{l}^\pm \rightarrow l^\pm \tilde{\chi}_1^0$  would be softer. This in turn would reduce the trilepton detection efficiency. Consequently, the limit on  $m_{\tilde{\chi}_1^0}$  for a fixed  $m_{\tilde{\chi}_1^\pm}$  may decrease by 10-25 GeV compared to Fig.1(a). In regard to the cold dark matter results in Fig.2(a), the annihilation/coannihilation properties of LSP are almost unchanged from the LGLS scenario. However, this scenario is in tension with the  $\Delta a_\mu$  constraint at  $2\sigma$  level.

The direct slepton search limits also disallow a large part of the parameter space which is allowed by the trilepton searches. In fact the bottom limb of the relic density satisfied region corresponding to LSP pair annihilation into the  $h$ -resonance is disfavoured even if the  $(g-2)_\mu$  constraint is relaxed to  $3\sigma$ .

In Fig.2(b), we consider  $\tan\beta = 30$ . The results in regard to DM production via LSP - sneutrino coannihilation and  $(g-2)_\mu$  studies are similar to what has been described for Fig.1(b) for the reasons discussed above. On the other hand, with large  $\tan\beta$  and for small values of  $M_2$  the parameter region in the  $(m_{\tilde{\chi}_1^\pm} - m_{\tilde{\chi}_1^0})$  plane where DM pair-annihilation into the  $h$ -resonance could possibly occur as in Fig.1(b) is already excluded here because sneutrinos turn out to be the LSP or even tachyonic. In regard to muon anomaly, Fig.2(b) shows an agreement even up to  $1\sigma$  level. The nature of the two discarded cyan regions is similar to those of Fig.2(a), but the shape of the lower discarded region depends on the choice of the scale in the radiative electroweak symmetry breaking (REWSB) conditions [3]. We have employed the canonical choice of the scale as the geometric mean of the two top-squark scalar mass parameters.

## ii) LGLS- $\tilde{\chi}_1^\pm$ :

In the analysis leading to Fig.3(a) we use  $x = 0.25$ . Thus, here L-sleptons are closer in mass with that of  $\tilde{\chi}_1^\pm/\tilde{\chi}_2^0$ . As a result the leptons arising from decays via  $\tilde{\chi}_1^\pm \rightarrow l^\pm \tilde{\nu}$  or  $\tilde{\chi}_2^0 \rightarrow \tilde{l}^\pm l^\mp$  would be softer. This would reduce the trilepton efficiency and relax the LHC constraints. Compared to Fig.1(a) we find that the limit on  $m_{\tilde{\chi}_1^0}$  relaxes by 20-40 GeV which allows the parameter space to become available at  $1\sigma$  limit of the  $(g-2)_\mu$  constraint. Consequently, parameter points corresponding to low mass sparticles with masses as low as  $m_{\tilde{\chi}_1^\pm} \simeq 135$  GeV and  $m_{\tilde{\chi}_1^0} \simeq 100$  GeV in Fig.3(a) become allowed. DM relic density production is driven by sneutrino-LSP coannihilation in the parameter space consistent with LHC and  $(g-2)_\mu$  constraints. Fig.3(b) shows the result for  $\tan\beta = 30$ . Here satisfying DM constraint by the Higgs resonance is disfavoured for reasons

similar to what was described for Fig.1(b).

We also note that depending on  $M_1$  and  $M_2$ , situations may arise when the masses of the sleptons with positive D-term contributions may become larger than  $m_{\tilde{\chi}_1^\pm}$  or  $m_{\tilde{\chi}_2^0}$ , but the sneutrinos which have negative D-term contributions for their masses, may become lighter than the above gauginos. Then,  $\tilde{\chi}_2^0$  decays into neutrino-sneutrino pairs with large BRs (100%). The latter in turn would undergo invisible decay into neutrino and the LSP. In each LGLS- $\tilde{\chi}_1^\pm$  scenario there is a value of  $x$  which will deplete the trilepton signal due to such blind spots. Because of the above there are several blind spots in Figs.3(a) and 3(b). This scenario with three invisible sparticles (the LSP,  $\tilde{\chi}_2^0$  and the sneutrino) have interesting collider phenomenology [74,75]. In particular at a high energy  $e^+e^-$  collider [76] it would lead to a significantly enhanced signal in the single photon + missing energy channel [77] compared to a pMSSM scenario with LSP as the lone carrier of missing energy [78].

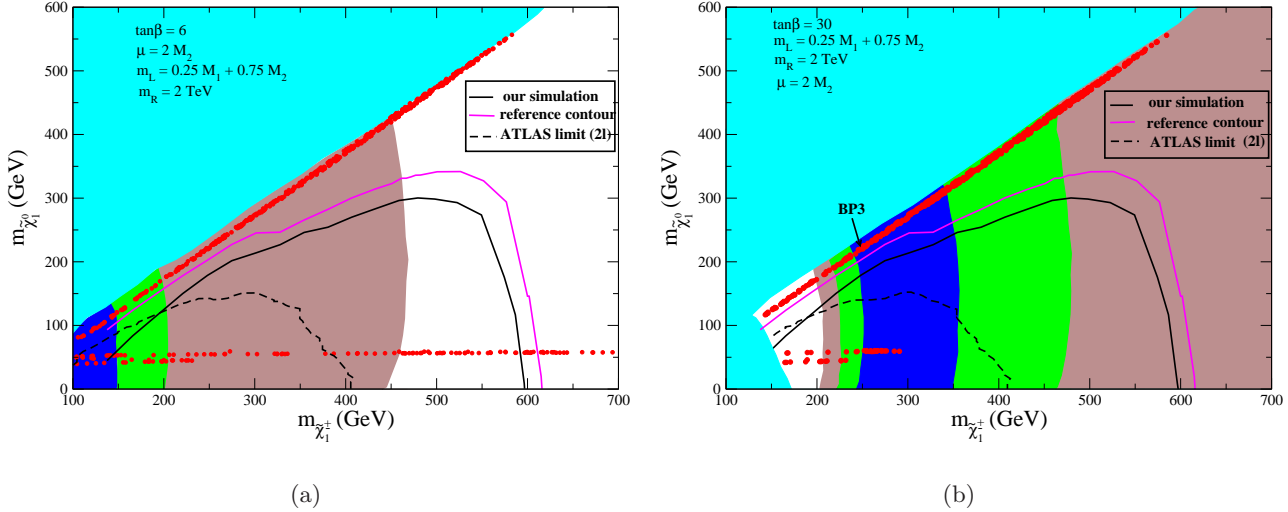


Figure 3: (a) Plot in the  $m_{\tilde{\chi}_1^\pm} - m_{\tilde{\chi}_1^0}$  plane for the tilted LGLS scenario choosing  $M_{\tilde{L}} = 0.25M_1 + 0.75M_2$  and  $\tan\beta = 6$  (a) and 30 (b). Colours and conventions are the same as in Fig.1. The lightly shaded (cyan) upper region is discarded by the requirement of the LSP to be the lightest neutralino. The exclusion contour for this scenario is represented by black line.

### 3.2 Light Gaugino and Light Left and Right Slepton (LGLRS) Scenario

We now come to the analyses of the LGLRS scenario. This was not considered by the ATLAS collaboration [15]. We assume the R-slepton mass parameters ( $M_{\tilde{L}_R}$ ) to be same as that of the

L-sleptons ( $M_{\tilde{l}_L}$ ). The principal difference of this scenario with LGLS is that the L-R mixing effect becomes prominent in the third generation slepton sector. As a result the  $\tilde{\tau}_1$  instead of the sneutrino often becomes a charged NLSP or even the LSP leading to a forbidden region. For a given value of  $m_{\tilde{\chi}_1^\pm}$  this results into elimination of larger values of  $m_{\tilde{\chi}_1^0}$ , causing a shrinkage of parameter space for the upper  $m_{\tilde{\chi}_1^0}$  region in comparison to a corresponding LGLS case. There is a significant region in the smaller  $m_{\tilde{\chi}_1^0} - m_{\tilde{\chi}_1^\pm}$  zone that is discarded due to the appearance of tachyonic stau or stau becoming the LSP.

We start with the case of slepton mass parameters (L and R) at the average of  $M_1$  and  $M_2$  as in Fig.4(a). In regard to the DM relic density the upper branch arises via LSP-stau coannihilation and some bulk annihilations for low mass regions. The lower branch as usual occurs due to the  $h$ -resonance and some Z-resonance as well as some bulk-annihilations for the low mass regions.

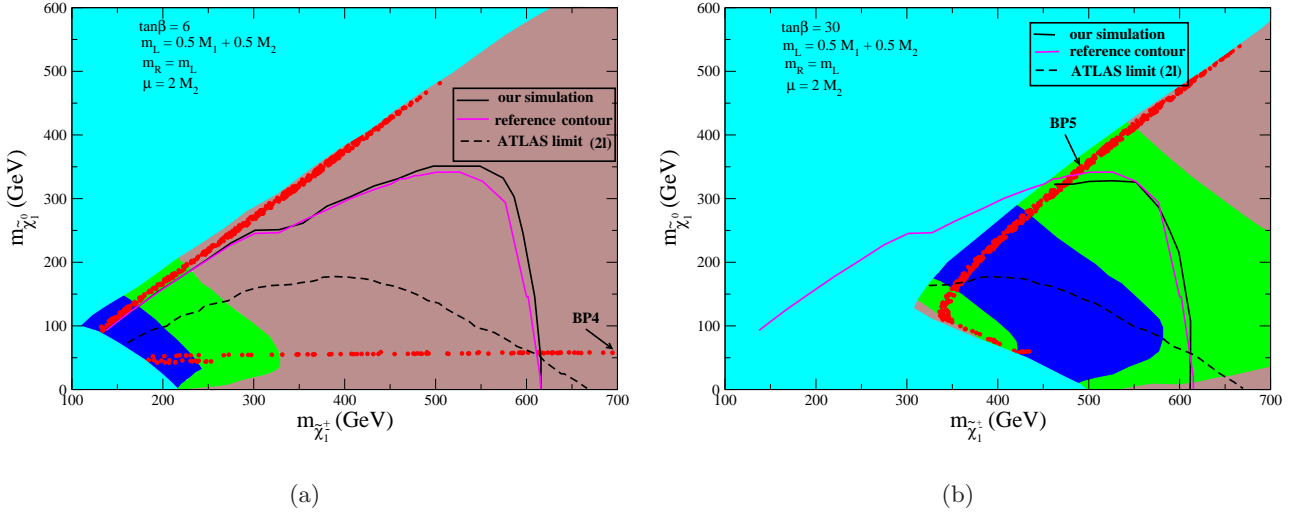


Figure 4: (a) Plot in the  $m_{\tilde{\chi}_1^\pm} - m_{\tilde{\chi}_1^0}$  plane for the LGLRS scenario with  $M_{\tilde{l}_L} = M_{\tilde{l}_R} = 0.5 M_1 + 0.5 M_2$  and  $\tan\beta = 6$  (a) and 30 (b). Colours and conventions are the same as in Fig.1. The exclusion contour for this scenario is represented by the black line.

Since both  $\tilde{\chi}_1^\pm$  and  $\tilde{\chi}_2^0$  are wino dominated, they primarily decay into left sleptons. Thus the inclusion of right sleptons does not alter BR of  $\tilde{\chi}_1^\pm$  and  $\tilde{\chi}_2^0$  decaying into left sleptons. But as the trilepton efficiency increases, the collider limit on  $m_{\tilde{\chi}_1^0}$  becomes stronger by 20-30 GeV for  $m_{\tilde{\chi}_1^\pm} > 450$  GeV compared to the reference contour of Fig.1(a). On the other hand, since

a part of neutralino-smuon loop contribution scales as  $\frac{m_\mu^2 M_{1\mu}}{M_{\tilde{\mu}_L}^D M_{\tilde{\mu}_R}^D} \tan\beta$  [45],  $a_\mu^{\text{SUSY}}$  is significantly boosted because both the left and the right slepton mass parameters are the same (unlike the LGLS scenario). A larger  $a_\mu^{\text{SUSY}}$  does not however make more and more smaller mass region in the  $m_{\tilde{\chi}_1^\pm} - m_{\tilde{\chi}_1^0}$  plane to be finally available. Much of such low mass regions become unavailable because  $\tilde{\tau}_1$  turns out to be lighter than the LSP due to L-R mixing or even it can become tachyonic. The unavailable regions fall in the cyan shaded zone. We must however keep in mind that an effort to nullify the L-R mixing by considering an appropriate non-vanishing  $A_\tau$  parameter would open up the low mass region that would also satisfy the constraints of collider and the WMAP/PLANCK data as well as  $(g-2)_\mu$  in this LGLRS scenario.

An analysis for  $\tan\beta = 30$  is presented in Fig.4(b). Here in comparison with Fig.1(b) the effects of L-R mixing (leading to unacceptably light  $\tilde{\tau}_1$ ) is significantly strong causing an appreciable shrinkage of the available parameter space.  $a_\mu^{\text{SUSY}}$  is enhanced due to a large value of  $\tan\beta$ . As before  $\tilde{\chi}_1^0 - \tilde{\tau}_1$  coannihilation is the dominant DM producing mechanism. The mechanism via h-resonance occurs in a region forbidden by unacceptable  $\tilde{\tau}_1$  mass. The lowest mass combination within the valid parameter space is about  $m_{\tilde{\chi}_1^\pm} \simeq 470$  GeV and  $m_{\tilde{\chi}_1^0} \simeq 330$  GeV that falls in the  $2\sigma$  zone of  $(g-2)_\mu$ .

### 3.2.1 Tilted LGLRS Scenario

#### i) LGLRS- $\tilde{\chi}_1^0$ :

In Fig.5(a) we explore the case where both L and R-sleptons are closer to the mass of the LSP via  $M_{\tilde{l}_L} = M_{\tilde{l}_R} = 0.75M_1 + 0.25M_2$ . While sleptons become light, similar to what happens for Fig.4(a) the dominant contribution to  $a_\mu^{\text{SUSY}}$  comes from the one-loop neutralino-smuon loop diagram as discussed before. As a result  $m_{\tilde{\chi}_1^\pm}$  becomes unconstrained leading to increase of the upper limit of the same for a given error corridor of  $(g-2)_\mu$  compared to what appears in Fig.4(a). In this case, as discussed before, the trilepton efficiency would decrease due to the fact that the sleptons are shifted more towards the LSP. Here it almost overlaps with the limit corresponding to Fig.1(a). Additionally, there is a large discarded region where  $\tilde{\tau}_1$  becomes the LSP or tachyonic because of mixing between the components of the third generation of slepton fields. The allowed region satisfying the relic density constraint and the collider limits mostly occurs in the  $3\sigma$  region of  $(g-2)_\mu$ . We note that the direct slepton mass bounds from ATLAS disallow the entire bottom

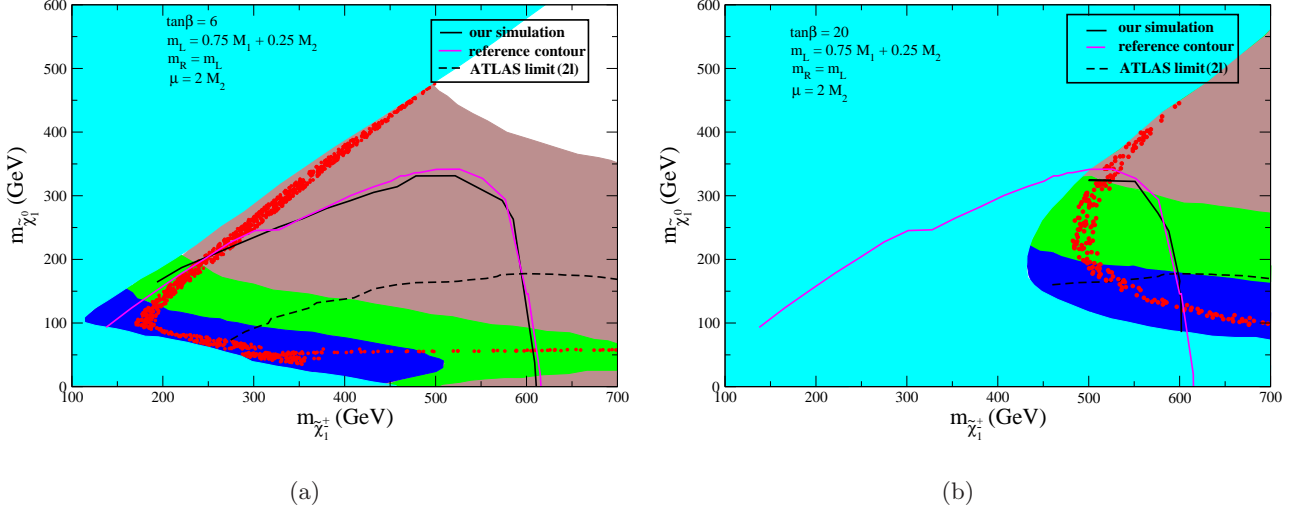


Figure 5: (a) Plot in the  $m_{\tilde{\chi}_1^\pm} - m_{\tilde{\chi}_1^0}$  plane for the LGLRS scenario with  $M_{\tilde{L}} = M_{\tilde{R}} = 0.75M_1 + 0.25M_2$  and  $\tan\beta = 6$  (a) and 20 (b). Colours and conventions are same as Fig.1. The exclusion contour for this scenario is represented by the black line.

limb of the relic density satisfied region that is associated with the  $h$ -pole annihilation unless  $m_{\tilde{\chi}_1^\pm}$  is very large. Thus we do not find any APS in this scenario if the  $(g-2)_\mu$  constraint is imposed at the level of  $2\sigma$ .

In Fig.5(b), we are compelled to use a relatively smaller value of  $\tan\beta$  ( $= 20$ ) unlike previous results, where we could comfortably analyse a larger value of  $\tan\beta$  ( $= 30$ ). This is simply because, in this case the slepton masses are closer to the LSP mass and the masses of the left and right slepton partners are almost similar in magnitude (apart from D-term contributions). The effect of mixing is dominant in the stau sector and this leads to  $\tilde{\tau}_1$  to become the LSP or even tachyonic for a larger value of  $\tan\beta$ . Even for  $\tan\beta = 20$ , as may be seen in Fig.5(b) there is a considerable region that becomes discarded because of the above reason. The collider limits on the other hand remain almost unchanged with respect to that of Fig.5(a).

The dominant diagrams contributing to  $a_\mu^{\text{SUSY}}$  are the neutralino-smuon loop diagrams similar to the other LGLRS models. Here, the regions allowed via  $(g-2)_\mu$  that also satisfy the collider limits and the DM relic density occur i) in the  $3\sigma$  zone for which the mass of LSP is higher and ii) in the  $1\sigma$  zone for which the mass of  $\tilde{\chi}_1^\pm$  is higher ( $> 600$  GeV). The DM relic density satisfied points result mainly from LSP- $\tilde{\tau}_1$  and  $\tilde{\tau}_1 - \tilde{\tau}_1$  coannihilations in the upper zone. In the lower region there are some points for which the LSP undergoes self-annihilations via t-channel slepton exchange

mechanism thus producing the right amount of abundance. The importance of the direct slepton search is showcased by this scenario. It rules out the LGLRS- $\tilde{\chi}_1^0$  model for high  $\tan\beta$  discussed above, which is consistent with  $(g-2)_\mu$ , WMAP/PLANCK data and trilepton searches at the LHC.

ii) **LGLRS- $\tilde{\chi}_1^\pm$** :

Fig.6(a) describes the constraints in a scenario with the common slepton mass parameter closer to  $m_{\tilde{\chi}_1^\pm}$  ( $M_{\tilde{l}_L} = M_{\tilde{l}_R} = 0.25M_1 + 0.75M_2$ ) for  $\tan\beta = 6$ . The dominant corrections contributing to  $a_\mu^{\text{SUSY}}$  come from the neutralino-smuon loop diagrams similar to other cases of small left and right slepton masses. Since the slepton masses are closer to  $m_{\tilde{\chi}_1^\pm}$  than  $m_{\tilde{\chi}_1^0}$ , the trilepton efficiency decreases. This weakens the collider limit of  $m_{\tilde{\chi}_1^0}$  by 15-45 GeV compared to the reference contour. As seen from the figure this shrinkage of limit in turn opens up a parameter space to the  $(g-2)_\mu$  constraint at  $1\sigma$  level. The DM relic density satisfying mechanisms are annihilations via s-channel Higgs resonance and some t-channel slepton exchange for a small  $m_{\tilde{\chi}_1^\pm}$  for the lower horizontal branch of red points only. This branch is, however, strongly disfavoured by the LHC data. For the upper branch, the relic density is satisfied via a multitude of processes like LSP annihilations via chargino mediation and various coannihilations such as those between LSP-stau, LSP-sneutrino, stau-stau, stau-sneutrino, sneutrino-sneutrino, and chargino-sneutrino.

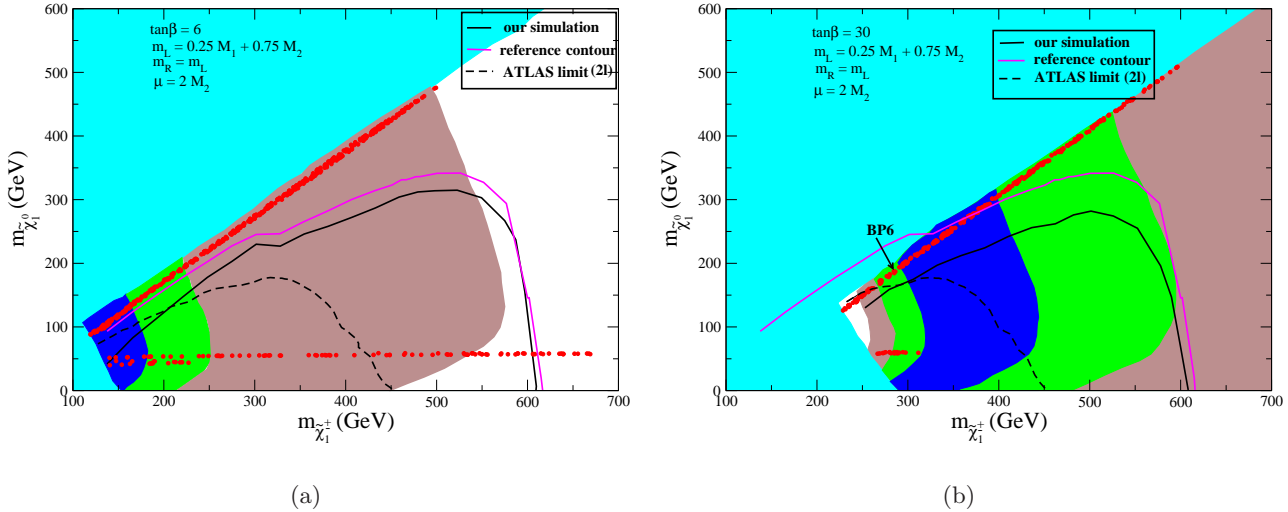


Figure 6: (a) Plot in the  $m_{\tilde{\chi}_1^\pm} - m_{\tilde{\chi}_1^0}$  plane for the LGLRS scenario with  $M_{\tilde{l}_L} = M_{\tilde{l}_R} = 0.25M_1 + 0.75M_2$  and  $\tan\beta = 6$  (a) and 30 (b). Colours and conventions are same as Fig.1. The exclusion contour for this scenario is represented by the black line.



Fig.6(b) refers to  $\tan\beta = 30$ . The  $(g-2)_\mu$  allowed regions are extended to larger values of  $M_2$ . The trilepton efficiency is smaller here even in comparison with Fig.6(a). This is due to the fact that there is a large mixing in the stau sector leading to an increase in the branching ratio of  $\tilde{\chi}_1^\pm/\tilde{\chi}_2^0$  decaying into  $\tilde{\tau}_1$ , which in turn decreases the number of trilepton events. The combined effect weakens the collider limit upto 65-75 GeV for most of the parameter space. The DM relic density satisfying mechanisms for the upper branch are mainly LSP- $\tilde{\tau}_1$  and  $\tilde{\tau}_1$ - $\tilde{\tau}_1$  coannihilations. For the tiny lower branch there is not much difference with the situation encountered earlier for large  $\tan\beta$ .

### 3.3 Light Gaugino and Right Slepton (LGRS) Scenario

In this case, we consider the R-slepton mass for all the three generations to lie between  $m_{\tilde{\chi}_1^0}$  and  $m_{\tilde{\chi}_1^\pm}$  so that  $M_{\tilde{l}_R} = \frac{1}{2}(M_1 + M_2)$ . The corresponding L-slepton mass parameter is taken to be greater than the lighter chargino mass:  $M_{\tilde{l}_L} = M_2 + 200$  GeV. Fig.7 shows the results for the

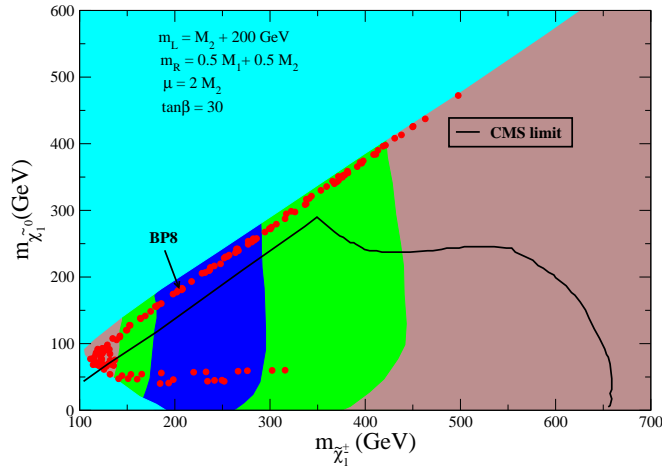


Figure 7: Result of scanning the  $m_{\tilde{\chi}_1^0}$ - $m_{\tilde{\chi}_1^\pm}$  plane for the LGRS scenario with  $\tan\beta = 30$ . Here,  $M_{\tilde{l}_L} = M_2 + 200$  GeV, and  $M_{\tilde{l}_R} = 0.5M_1 + 0.5M_2$ . Colours and conventions are same as those of Fig.1. The CMS exclusion contour is shown as a black line (Fig.21 of Ref. [17]).

LGRS scenario with  $\tan\beta = 30$ . The CMS exclusion contour (Fig.21 of Ref. [17]) is shown as a black line. The main contribution to  $a_\mu^{\text{SUSY}}$  comes from the neutralino-smuon loop. For moderate

values of  $M_2$ , the contribution coming from the chargino-sneutrino (bino-higgsino- $\tilde{\mu}_R$ ) loop is also significant.

The PLANCK/WMAP allowed points for the upper branch undergo LSP-stau, as well as stau-stau coannihilations. However, the region at the lower end of this branch corresponding to bulk annihilation is disfavoured by the  $(g-2)_\mu$  data. There also exists a small amount of coannihilation of LSP/stau with the right handed slepton of the first two generations and annihilations via chargino exchange. For the lower branch disfavoured by the LHC data, there are resonant Higgs/Z exchange annihilation processes and also bulk annihilation. As can be seen from the figure, there is a significant area of parameter space which satisfies WMAP/PLANCK data,  $(g-2)_\mu$  at the level of  $1\sigma$  along with collider constraints.

### 3.4 Light Gaugino and Heavy Slepton (LGHS) Scenario

The ATLAS group has also searched for the trilepton signal in the light gaugino heavy slepton (LGHS) model. All sleptons with equal masses for the left and the right components are assumed to be heavier than  $\tilde{\chi}_1^\pm$  or  $\tilde{\chi}_2^0$ . The bounds mainly depend on the chargino and the LSP mass

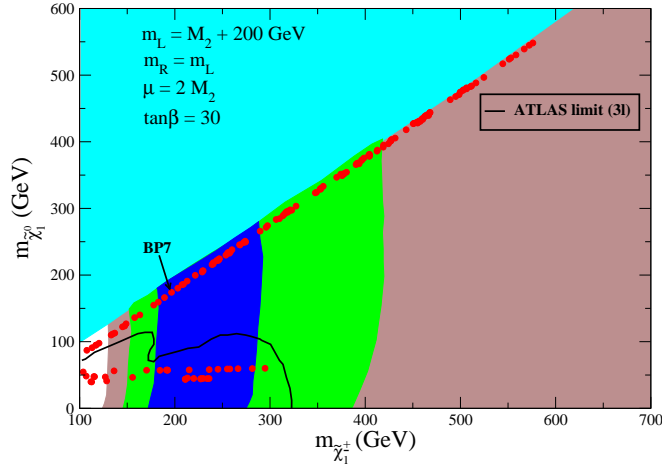


Figure 8: Plot in the  $m_{\tilde{\chi}_1^\pm} - m_{\tilde{\chi}_1^0}$  plane for the LGHS scenario with  $M_{\tilde{l}_R} = M_{\tilde{l}_L} = M_2 + 200$  GeV and  $\tan\beta = 30$ . Colours and conventions are same as Fig.1. The black line represents the exclusion contour at 8 TeV by the ATLAS collaboration [15].

(see the exclusion contour in Fig.8b of ATLAS [16] reproduced in Fig.8 for ready reference). The sensitivity to the other MSSM parameters is rather mild.

We consider the representative choice  $M_{\tilde{l}_R} = M_{\tilde{l}_L} = M_2 + 200$  GeV as in Fig.8. It may be noted that with this choice the sleptons contribute neither to the LHC signal nor do they affect LSP annihilation/coannihilation. Here, since  $\tilde{\chi}_1^\pm$  or  $\tilde{\chi}_2^0$  are unable to decay into sleptons, they decay via gauge bosons with a 100% branching ratio. As a result, each collider limit becomes independent of the SUSY input parameters like  $\tan\beta$ . Here the choice  $\tan\beta = 30$ , simply yields a large  $a_\mu^{\text{SUSY}}$  leading to widening of the  $1\sigma$  allowed region for  $(g-2)_\mu$  (the dominant contributions to  $a_\mu^{\text{SUSY}}$  come from the neutralino-smuon loops)<sup>13</sup>. The relic density producing mechanisms for the lower red points are annihilations via s-channel Higgs and Z resonances which are disfavoured by the LHC data. Points in the upper branch primarily undergo  $\tilde{\chi}_1^\pm/\tilde{\chi}_2^0$  coannihilations.

In obtaining the LHC exclusion contour in Fig.8 it is assumed that the decay  $\tilde{\chi}_2^0 \rightarrow Z\tilde{\chi}_1^0$  occurs with 100% BR. However, in parts of the excluded parameter space, the spoiler mode  $\tilde{\chi}_2^0 \rightarrow h\tilde{\chi}_1^0$  may occur with significant BR and weaken the limits [50]. It is particularly interesting to note that in the Higgs resonance region the BR of this mode is appreciable for  $m_{\tilde{\chi}_1^\pm} \approx m_{\tilde{\chi}_2^0} > m_h + m_{\tilde{\chi}_1^0} \approx 1.5m_h$ . As a result this region, particularly the points close to the exclusion contour, cannot be excluded beyond doubt. On the other hand the exclusion obtained by assuming that  $\tilde{\chi}_2^0 \rightarrow h\tilde{\chi}_1^0$  occurs with 100% BR is too weak to affect the Higgs resonance region [50].

### 3.5 Light Left Slepton (LLS) Scenario

In the Light Left Slepton model, the left sleptons are light but the right sleptons and all the charginos and the neutralinos except the LSP are heavy. The ATLAS collaboration has reported the results of slepton search in the LLS model [16]. Their exclusion contour is reproduced in Fig.9.

With the choice of a heavy right slepton ( $M_{\tilde{l}_R} = 1$  TeV), we scan  $M_1$  and  $M_{\tilde{l}_L}$  and show the results in the  $m_{\tilde{\chi}_1^0} - M_{\tilde{l}_L}^D$  plane of Fig.9. We fix a wino dominated lighter chargino with the choice of  $M_2 = 800$  GeV and  $\mu = 1$  TeV for  $\tan\beta = 30$ . This choice of  $M_2$  is motivated by the chargino mass bounds in the LGLS models considered in Sec. 3.1.  $M_1$  is varied upto 600 GeV for the given choice of  $M_2$  and  $\mu$  so as to have a bino-like LSP. With the right slepton being heavy,

---

<sup>13</sup>For  $\tan\beta = 6$  LSP pair annihilation via Higgs resonance would be quite efficient but consistency of  $a_\mu^{\text{SUSY}}$  with the measured value is only at the  $3\sigma$  level.

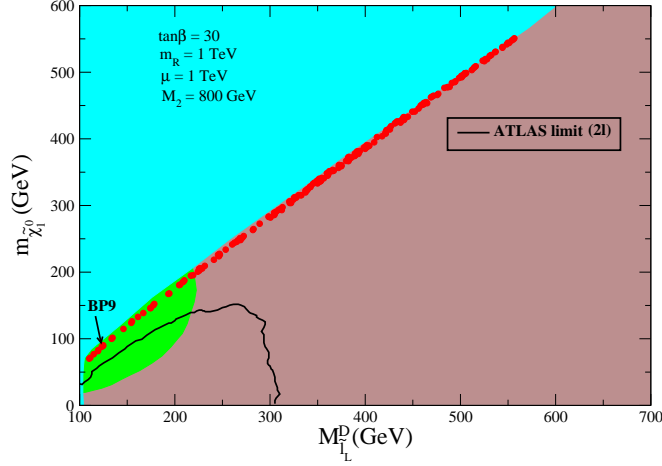


Figure 9: Plot in the  $M_{\tilde{L}}^D - m_{\tilde{\chi}_1^0}$  plane for the LLS scenario with  $M_2 = 800$  GeV,  $\mu = 1$  TeV and  $\tan\beta = 30$ . Here  $M_{\tilde{L}}^D$  represents physical left slepton masses. Colours and conventions are same as those of Fig.1. The black line represents the exclusion contour at 8 TeV by the ATLAS collaboration [16].

the contribution from neutralino-smuon loop to  $a_\mu^{\text{SUSY}}$  is suppressed. Again, since  $\mu$  and  $M_2$  are sufficiently large in magnitude, the chargino-sneutrino loop is also suppressed. Nevertheless, we have acceptable  $a_\mu^{\text{SUSY}}$ , though at the  $2\sigma$  level, consistent with all other constraints. The red points satisfy DM relic density constraint by primarily LSP-sneutrino coannihilations. There are also sneutrino-sneutrino, sneutrino-stau coannihilations.

### 3.6 Light Left and Right Slepton (LLRS) Scenario

Here the right and the left sleptons are assumed to be degenerate in mass and are lighter than the lighter chargino (Fig.10). The ATLAS collaboration has also reported slepton pair production in the LLRS model in addition to LLS [16].

Since the  $\tilde{\chi}_1^\pm$  and  $\tilde{\chi}_2^0$  are taken to be heavier than the sleptons, the sleptons decay into leptons and  $\tilde{\chi}_1^0$  with 100% branching ratio. Thus, the exclusion limits would be independent of the input parameters like  $M_2$ ,  $\mu$ ,  $\tan\beta$  etc. Here we use the ATLAS exclusion contour [16] as shown in Fig.10. Fig.10(a) shows the results for the case of light and degenerate left and right sleptons ( $M_{\tilde{L}} = M_{\tilde{R}}$ ) for  $\tan\beta = 6$ . There is a significant amount of parameter space which is allowed by the collider

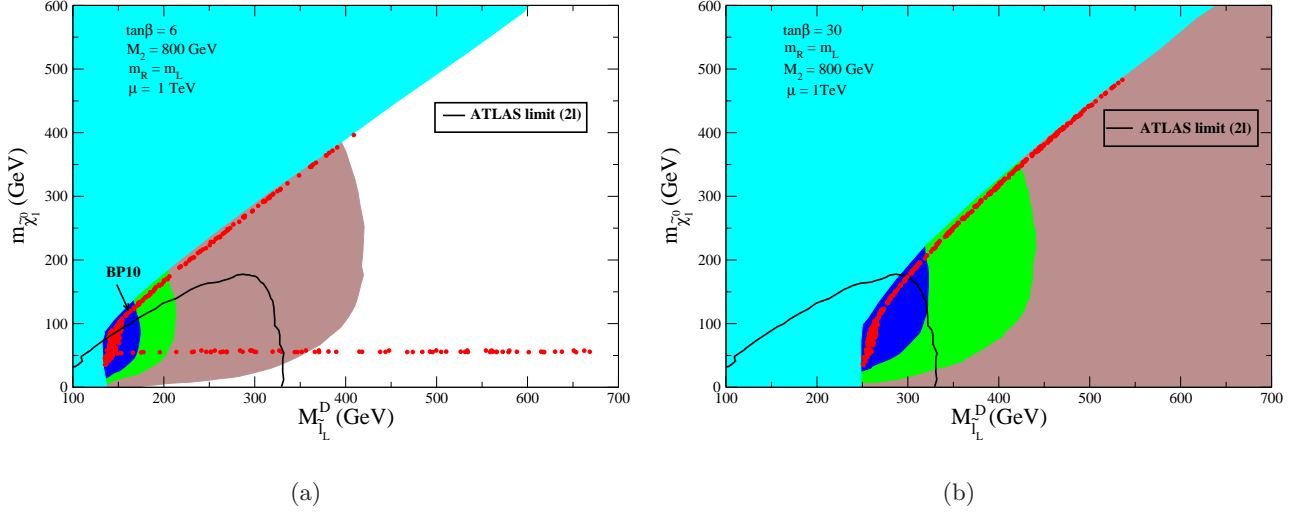


Figure 10: (a) Plot in the  $M_{\tilde{l}_{L/R}}^D - m_{\tilde{\chi}_1^0}$  plane for the LLRS scenario with  $M_2 = 800$  GeV and  $\tan\beta = 6$  (a) and 30 (b). The common masses of sleptons are varied so that these are always smaller than  $m_{\tilde{\chi}_1^\pm}$ . Colours and conventions are same as those of Fig.1. The black line represents the exclusion contour at 8 TeV by the ATLAS collaboration [16].

data and  $(g - 2)_\mu$  constraint at the level of  $1\sigma$ . The principal contributions to  $a_\mu^{\text{SUSY}}$  come from the neutralino-smuon diagrams. The DM relic density satisfying mechanisms for the upper branch are LSP-stau coannihilations. The s-channel light Higgs resonance process is viable only if  $M_{\tilde{l}_L} = M_{\tilde{l}_R} > 360$  GeV. However, for this region  $a_\mu^{\text{SUSY}}$  is satisfied only at the level of  $3\sigma$  for a narrow range of slepton masses. At the lower left corner of the parameter space, there is a nearly vertical strip of DM relic density satisfied points with low values of input slepton mass. Only a small part of this region corresponding to bulk annihilation is allowed by the LHC data.

In Fig.10(b) we show a similar study with  $\tan\beta = 30$  that shows the effect of enhanced  $a_\mu^{\text{SUSY}}$  leading to opening of  $1\sigma$  region for larger values of the slepton masses. The region with  $M_{\tilde{l}_L} \leq 250$  GeV is discarded because here stau becomes the LSP. Similar to the case of  $\tan\beta = 6$ , there is a region with low values of slepton mass that arises because of bulk annihilation which is disfavoured by the LHC data. The upper red points satisfy relic density constraint through LSP-stau coannihilation.

## 4 Direct and Indirect Detections of Dark Matter

### 4.1 Direct Detection

We probe the direct search prospects of dark matter for the scenarios discussed above keeping in mind the uncertainties stated in Sec. 2.3. The spin independent scattering of the LSP with a proton may occur via t-channel Higgs exchange or s-channel squark exchange processes. Since the squarks are very heavy in view of the LHC bounds, the Higgs exchange processes would dominantly contribute to  $\sigma_{\chi p}^{\text{SI}}$ . However, since we consider only a bino-like LSP, we do not expect the scattering cross-section to be too large [63]. In the following figures we only show the points which satisfy PLANCK/WMAP constraint,  $(g-2)_\mu$  data upto the level of  $2\sigma$  and collider limits.

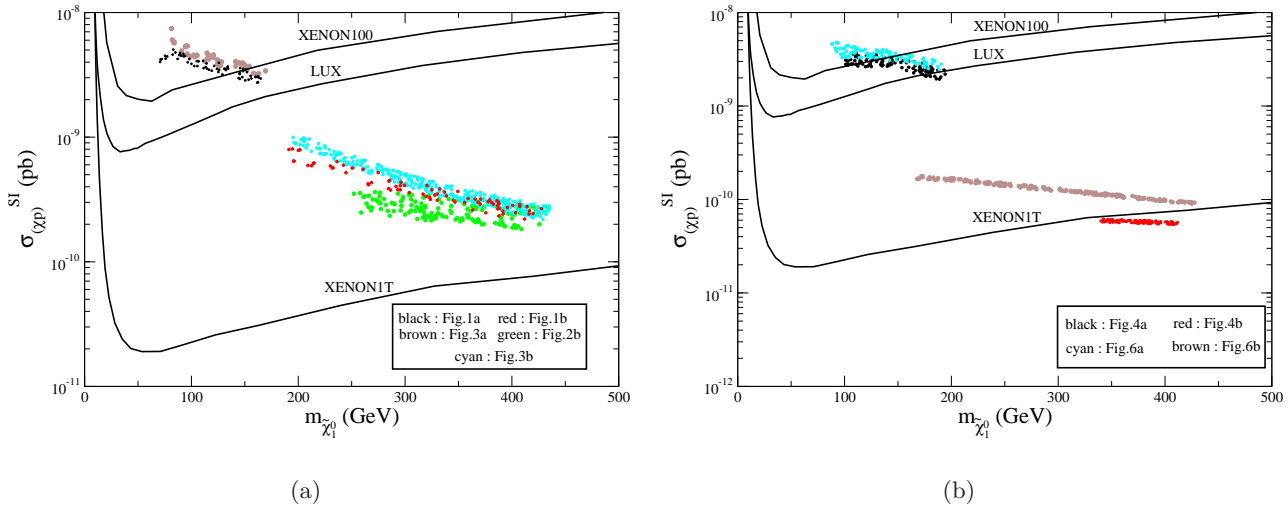


Figure 11: (a) Plot of spin independent scattering cross-section  $\sigma_{\tilde{\chi}_1^0 p}^{\text{SI}}$  for scattering of proton with  $\tilde{\chi}_1^0$  as a function of the mass of the LSP for the LGLS scenarios. Only the points which satisfy WMAP/PLANCK,  $(g-2)_\mu$  upto the level of  $2\sigma$  and collider constraints are shown in the figure. The exclusion contours for XENON100, LUX and XENON1T experiments are shown as black lines. Black and red points represent the case of Fig.1(a) and Fig.1(b) respectively. Green, brown and cyan points represent the case of Fig.2(b), Fig.3(a) and Fig.3(b) respectively. (b) Similar plot as (a) for the LGLRS scenarios. Black, Red, cyan and brown points represent the cases of Fig.4(a), 4(b), 6(a) and 6(b) respectively.

In Fig.11(a) we plot  $\sigma_{\chi p}^{\text{SI}}$  vs the mass of LSP for the LGLS scenarios (see Sec. 3.1) using

micrOMEGAs (version 3.2) [66]. The exclusion limits specified by the present XENON100 [21], LUX [22] and future XENON1T [23] experiments are shown as black lines. It follows from Sec. 3 that the tilted LGLS- $\tilde{\chi}_1^0$  model at low  $\tan\beta$  (Fig.2(a)) is excluded. Hence it does not appear in this figure. It also follows from Fig.11(a) that two other models at low  $\tan\beta$  namely the LGLS model (Fig.1(a)) and the tilted LGLS- $\tilde{\chi}_1^\pm$  model (Fig.3(a)) of Sec. 3.1 are disfavoured by the direct detection experiments. However, as discussed in Sec. 2,  $\sigma_{\tilde{\chi}p}^{\text{SI}}$  could have at least an order of magnitude of uncertainties. We therefore do not take the disfavoured points as finally excluded. We note that because of decreased coupling there is a significant reduction in cross-section while moving from  $\tan\beta = 6$  to  $\tan\beta = 30$ . We further note that the remainder of this class of models will be closely probed by XENON1T [23] experiment.

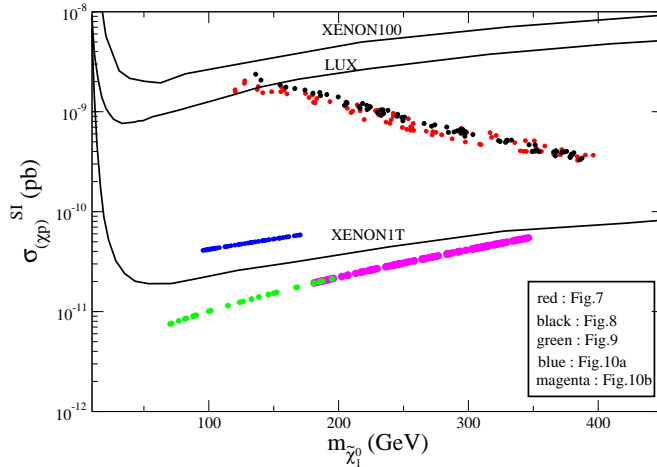


Figure 12: *Similar plot as Fig.11 for the scenarios described in Figs. 7 to 10. Red, black, green, blue and magenta points represent the cases of Figs.7, 8, 9, 10(a) and 10(b) respectively.*

Our results for the LGLRS scenarios (see Sec. 3.2) are shown in Fig.11(b). We note that Fig.5(a) and Fig.5(b) corresponding to tilted LGLRS- $\tilde{\chi}_1^0$  scenarios for low and high  $\tan\beta$  have already been disfavoured by the analysis of Sec. 3.2.1. Modulo the aforesaid uncertainties, the available points corresponding to LGLRS (Fig.4(a)) and tilted LGLRS- $\tilde{\chi}_1^\pm$  (Fig.6(a)) scenarios at low  $\tan\beta$  are disallowed via LUX [22] data. These models will be conclusively probed via the XENON1T. In addition, XENON1T will tightly scrutinize the remaining scenarios (LGLRS and

tilted LGLRS- $\tilde{\chi}_1^\pm$ ) at high  $\tan \beta$ .

The direct detection cross-section for all the other cases namely LGRS, LGHS, LLS and LLRS (see Fig.7 to Fig.10 ) are plotted in Fig.12. These models are fairly insensitive to XENON100 [21] and LUX [22] data. They can only probe the cases like LGHS and LGRS models for low mass range of LSP. The large  $m_{\tilde{\chi}_1^0}$  region of these models and the remaining models will be probed by the XENON1T. Moreover, some of the models can even be excluded if the theoretical uncertainties are brought under control in future.

## 4.2 Indirect Detection of DM through Photon Signal

Indirect detection of DM via photon signals may be useful for probing certain types of DM candidates. In general, weakly interacting massive particles (WIMP) may undergo nuclear scattering that would reduce the velocity of the WIMP leading to gravitational capture within dense regions of astrophysical objects such as the galactic center, dwarf galaxies or even the Sun or the Earth [26]. At tree level, WIMPs or LSPs may annihilate into fermion-antifermion pairs (quarks or leptons)

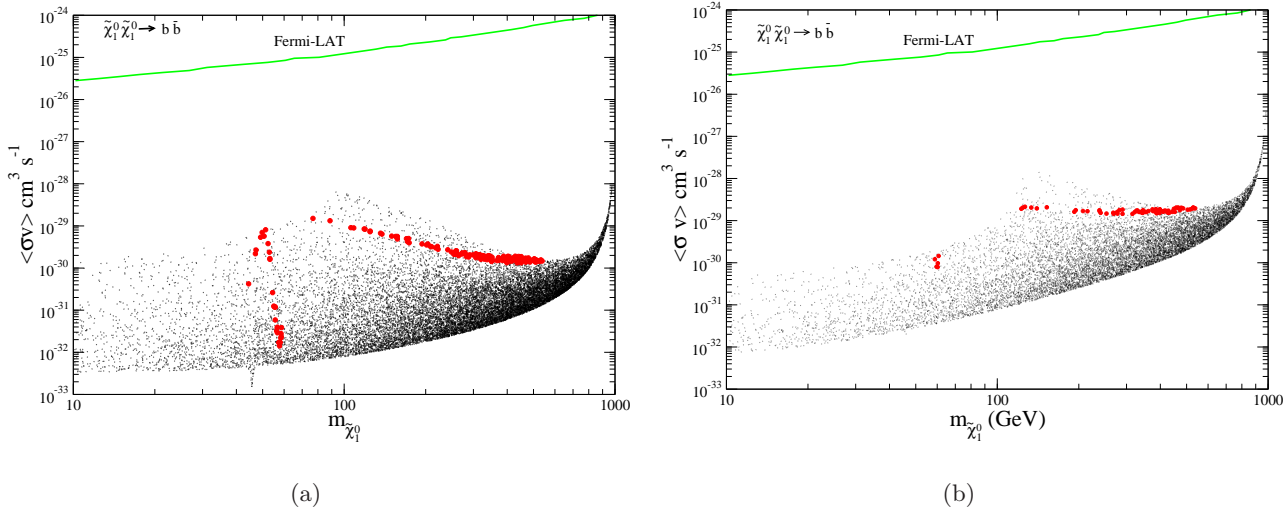


Figure 13: (a) Scatter plot of DM self-annihilation cross-section against LSP mass for the scenario described in Fig.1(a). The red points satisfy WMAP relic density constraint. Fermi-LAT exclusion limit for  $\tilde{\chi}_1^0 \tilde{\chi}_1^0 \rightarrow b \bar{b}$  channel is shown as a green line. (b) Similar plot as (a) for the case of Fig.1(b).

or Electroweak bosons. Hadronisation and decays of the product of primary annihilations may produce  $\pi^0$  that would lead to photons. This is apart from the photons belonging to the final state



radiation of primary particles. We note that unlike the annihilations that occurred at the freeze-out temperature when LSP would have a velocity that is an appreciable fraction of the speed of light  $c$ , in the present day environment of gravitational capture of LSPs the latter have a much smaller velocity  $v \sim 300$  km/s or  $v/c \sim 10^{-3}$  [79]. Thus, there is a large  $p$ -wave suppression ( $\sim (v/c)^2$ ) in the annihilation of the LSPs.

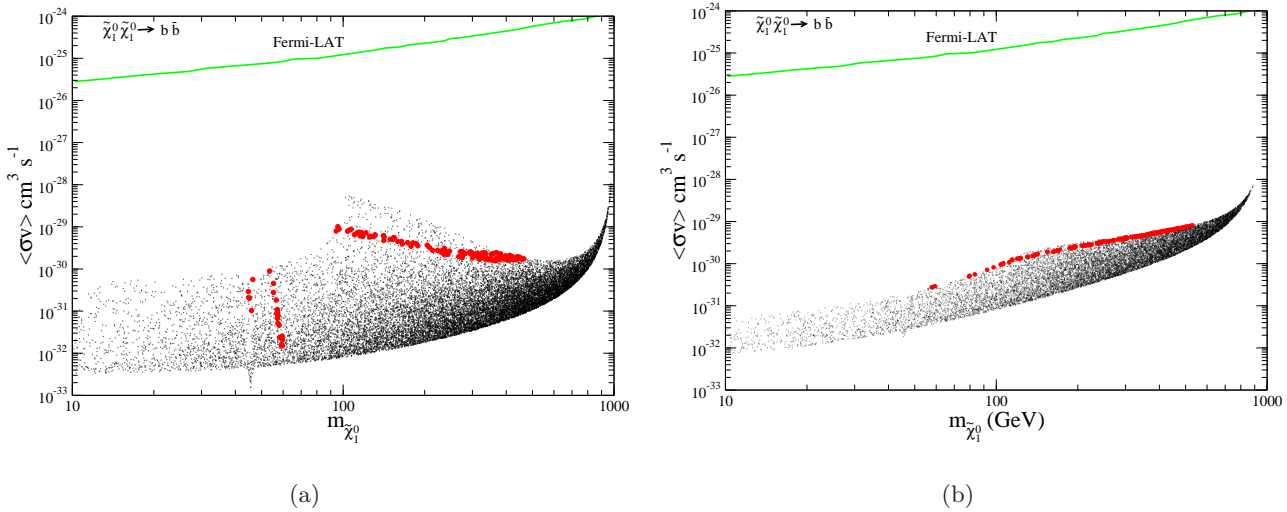


Figure 14: (a) Scatter plot of DM self-annihilation cross-section against LSP mass for the scenario described in Fig. 4(a). The red points satisfy WMAP relic density constraint. Fermi-LAT exclusion limit for  $\tilde{\chi}_1^0 \tilde{\chi}_1^0 \rightarrow b\bar{b}$  channel is shown as a green line. (b) similar plot as (a) for the case of Fig. 4(b).

On the other hand, with  $s$ -wave annihilation becoming the dominating mode there is a strong helicity suppression that disfavours light leptons/quarks in the final state. We note that for the combined  $s$ -wave state, the parity of the LSP-pair is negative. Neutralino being a Majorana particle (*i.e.* same as its anti-particle) the combined CP property of the LSP pair is same as the combined parity of the LSP-pair, which is negative. Hence one finds that the CP-odd Higgs boson resonance channel to contribute dominantly toward the photon signal. This can obviously increase if there is a sufficient higgsino component within the LSP. Thus with a principally bino type of LSP along with a large  $M_A$  (2 TeV) we do not expect any large photon signal for our models. Nevertheless, we compute the signal for two cases namely the LGLS scenarios (see Sec. 3.1, Fig. 1) and LGLRS scenarios (see Sec. 3.2, Fig. 4). We display the thermally averaged DM self-annihilation cross-section in Fig. 13 and Fig. 14. The results obtained by using micrOMEGAs (version 3.2) corresponds to the NFW

profile [80] for the DM density distribution. The Fermi-LAT exclusion bound for the above quantity [24] for the annihilation channel  $\tilde{\chi}_1^0 \tilde{\chi}_1^0 \rightarrow b\bar{b}$  corresponding to the given profile is as shown. The figures show that the cross-sections for our case stay way below the Fermi exclusion limits and there is a rise in cross-section when  $m_{\tilde{\chi}_1^0}$  goes close to  $M_A/2$ , as expected, from the discussion made above.

## 5 Gluino Mass Limits in Different Models and Their Characteristic Signatures

We now study the feasibility of distinguishing different pMSSM scenarios introduced in Sec. 3. For this purpose we assume the gluino to be light while all squarks are heavy. We derive the gluino mass limit in each scenario discussed in Sec. 3, using the ATLAS data on  $N_{BSM}$  (see below) in the generic  $n$ -leptons +  $m$ -jets +  $\cancel{E}_T$  channel [4–6] for  $n = 0, 1$  and  $2$  (the same sign dilepton (SSD) signal). The variation of each mass limit indicates the sensitivity of the corresponding scenario to the search channels. This motivates us to choose observables with different values of  $n$  which can potentially distinguish the models. In the process we also derive the most stringent limits on  $m_{\tilde{g}}$  in the above scenarios and compare them with the corresponding LHC limits on mSUGRA and other simplified models.

We essentially follow the procedure of Ref. [40] and introduce appropriate ratios of the cross-sections of channels characterized by different values of  $n$  and for  $m_{\tilde{g}}$  beyond the LHC limits. However, this analysis is based on recent data along with one more observable compared to Ref. [40]. It is worth recalling that these ratios are almost free from theoretical uncertainties like the choice of the QCD scale, the parton density function etc.

For illustrating our main points, we chose several benchmark points (BPs) representing different EW sectors. All points except one (see below), are consistent with the LHC constraints from EW sparticle searches, the WMAP/PLANCK data, the  $(g - 2)_\mu$  (at the level of  $2\sigma$ ) and LUX data for direct detection of DM. Table 1 contains the sparticle spectra and the values of different observables corresponding to the BPs. The decay modes relevant for the gluino signals for  $m_{\tilde{g}} = 1.2$  TeV and their branching ratios (BRs) are included in Table 2. It may be noted that in this table the BRs of the gluino do not add upto 100 % in all cases. This is due to the fact that in some scenarios

the gluino also decays into the heavier chargino and the heavier neutralinos with small but non-negligible BRs. However, all modes are taken into account while simulating the gluino decay signal. Similarly  $\tilde{\chi}_2^0$  decays into  $\tilde{\tau}_2$ , the heavier stau mass eigenstate, with  $\approx 7.0\%$  BR for BP4 and BP10 which is not shown in Table 2.

Benchmark Points	$M_1$ (GeV)	$M_2$ (GeV)	$m_{\tilde{\chi}_1^0}$ (GeV)	$m_{\tilde{\chi}_1^\pm}$ (GeV)	$m_{\tilde{\chi}_2^0}$ (GeV)	$M_{iL}^D$ (l = e, $\mu$ ) (GeV)	$M_{iR}^D$ (l = e, $\mu$ ) (GeV)	$m_{\tilde{\tau}_1}$ (GeV)	$M_\nu^D$ (GeV)	$\Omega_{\tilde{\chi}} h^2$	$\sigma_{SI}$ $\times 10^{-10}$ (pb)	$a_\mu^{\text{SUSY}}$ $\times 10^{-9}$
BP1 (Fig.1b)	240	262	232	266	267	255	2000	255	243	0.116	5.7	2.9
BP2 (Fig.2b)	248	289	240	298	299	263	2000	263	251	0.127	2.8	2.5
BP3(Fig.3b)	229	245	220	248	249	246	2000	245	233	0.109	8.1	3.4
BP4(Fig.4a)	63	682	61	695	695	374	374	355	366	0.137	1.9	0.3
BP5(Fig.4b)	357	478	350	491	491	420	420	354	413	0.098	0.7	1.3
BP6(Fig.6b)	193	281	187	287	286	263	263	197	251	0.125	1.6	3.6
BP7(Fig.8)	179	194	171	196	196	397	397	371	390	0.127	16.2	3.1
BP8(Fig.7)	190	206	183	208	208	408	203	194	401	0.108	13.1	2.8
BP9(Fig.9)	89	700	86	709	709	122	1000	109	95	0.111	0.1	1.4
BP10(Fig.10a)	124	800	120	799	799	163	163	129	145	0.121	0.5	2.0

Table 1: *The sparticle spectra corresponding to different benchmark points (BPs) chosen from Fig.1 to Fig.10.*

The BPs correspond to different DM producing mechanisms and mass hierarchies among the EW sparticles. The mass hierarchies determine the relevant BRs as well as the efficiencies of the kinematical cuts for isolating the desired signals from the backgrounds. Below we summarize the main features of the above BPs.

- For BP1 - BP3 and BP9  $\tilde{\nu}$  is the NLSP and  $\tilde{\nu} - \tilde{\chi}_1^0$  coannihilation is the main DM producing mechanism.
- LSP pair annihilation via the Higgs resonance is one of the DM relic density producing mechanism for BP 4. However, this point is consistent with the  $(g - 2)_\mu$  constraint at the level of  $3\sigma$  only.
- For BPs 4 - 6, 8 and 10  $\tilde{\tau}_1$  is the NLSP and is responsible for DM production via coannihilation with the LSP.
- For BP7  $\tilde{\chi}_1^\pm$  is the NLSP and along with  $\tilde{\chi}_2^0$  it efficiently coannihilates with the LSP.

Decay Modes	BP1	BP2	BP3	BP4	BP5	BP6	BP7	BP8	BP9	BP10
$\tilde{g} \rightarrow \tilde{\chi}_1^0 q \bar{q}$	9.3	9.5	9.3	50.6	17.1	10.4	8.0	8.2	76.1	75.2
$\rightarrow \tilde{\chi}_2^0 q q'$	22.5	22.4	22.3	16.7	27.7	23.5	18.3	18.9	8.5	8.8
$\rightarrow \tilde{\chi}_1^\pm q \bar{q}$	45.0	44.8	44.9	32.6	55.2	46.8	37.3	38.6	15.2	15.9
$\rightarrow \tilde{\chi}_2^\pm q \bar{q}$	12.4	12.7	12.4	-	-	10.4	18.6	17.6	-	-
$\tilde{\chi}_1^\pm \rightarrow \tilde{\chi}_1^0 q q'$	-	-	-	-	-	-	65.8	-	-	-
$\rightarrow \tilde{\chi}_1^0 \ell \nu_\ell$	-	-	-	-	-	-	34.2	-	-	-
$\rightarrow \tilde{\nu}_\tau \tau$	27.8	22.1	33.2	17.0	16.3	14.5	-	-	17.3	17.0
$\rightarrow \tilde{\tau}_1 \nu_\tau$	6.4	11.8	1.2	9.0	24.5	44.5	-	100	16.5	8.9
$\rightarrow \tilde{\tau}_2 \nu_\tau$	-	-	-	7.4	-	-	-	-	-	7.4
$\rightarrow \tilde{\nu}_l l$	53.8	43.2	63.6	34.0	32.2	28.2	-	-	33.8	34.0
$\rightarrow \tilde{l}_L \nu_l$	12.0	22.8	2.0	32.6	26.4	12.2	-	-	32.2	32.4
$\tilde{\chi}_2^0 \rightarrow \tilde{\chi}_1^0 \gamma$	-	-	-	-	-	-	15.0	-	-	-
$\rightarrow \tilde{l}_L^\pm l^\mp$	16.5	26.4	4.6	32.9	27.3	13.2	-	-	33.1	33.4
$\rightarrow \tilde{\nu}_l \bar{\nu}_l$	49.5	39.8	61.8	33.6	31.3	26.2	-	-	32.9	32.9
$\rightarrow \tilde{l}_R^\pm l^\mp$	-	-	-	-	-	-	-	13.0	-	-
$\rightarrow \tilde{\tau}_1^\pm \tau^\mp$	9.1	13.9	2.8	9.1	25.5	47.4	-	87.0	17.2	9.2
$\rightarrow \tilde{\tau}_2^\pm \tau^\mp$	-	-	-	7.4	-	-	-	-	-	7.6
$\rightarrow \tilde{\nu}_\tau \bar{\nu}_\tau$	24.8	19.9	30.8	16.8	15.7	13.1	-	-	16.6	16.5
$\rightarrow \tilde{\chi}_1^0 q \bar{q}$	-	-	-	-	-	-	85.0	-	-	-

Table 2: The BRs (%) of the dominant decay modes of  $\tilde{g}$  (for  $m_{\tilde{g}} = 1.2$  TeV),  $\tilde{\chi}_1^\pm$  and  $\tilde{\chi}_2^0$  for the benchmark points. Here  $l$  stands for  $e$  and  $\mu$ , but  $\ell$  denotes all three generations of leptons. All leptonic sparticles arising from the decays of the  $\tilde{\chi}_1^\pm$  and the  $\tilde{\chi}_2^0$  decay into their SM partner and the LSP with 100 % BR.

For BP1 - BP10 (except BP7) both  $\tilde{\chi}_1^\pm$  and  $\tilde{\chi}_2^0$  decay into two body channels involving all the three lepton generations (see Table 2). As a result, final states enriched with leptons -both charged and neutral, are obtained from gluino decays. However, the abundance of  $e$  and  $\mu$  in the final state varies from case to case. In the first three scenarios,  $\tilde{\chi}_2^0$  decays dominantly into the invisible mode  $\tilde{\nu}_l \nu_l$  or  $\tilde{\nu}_\tau \nu_\tau$ . The extreme example is provided by BP3 where the combined BR of the invisible decays is 92.6%. This weakens the trilepton signature. On the other hand for BP6 and BP8,  $\tilde{\tau}_1$

is the NLSP leading to gluino signatures with  $\tau$ -rich final states. Since  $\tau$  decays primarily into hadrons, the final states with  $e$  and/or  $\mu$  will be suppressed. In BP8 with heavy L-sleptons the final state is entirely  $\tau$ -dominated. BP7 represents a scenario where both L and R-type sleptons are heavy and  $\tilde{\chi}_1^\pm$  as well as  $\tilde{\chi}_2^0$  both decay dominantly via three body modes into hadronic channels leading to weaker mass limits from gluino searches requiring  $e$  and  $\mu$  in the final states.

We now summarise the ATLAS SUSY search results in the  $n = 0, 1$  and  $2$  (same sign dilepton(SSD)) channels. The ATLAS group has updated their result for SUSY search in the jets +  $\cancel{E}_T$  channel ( $n = 0$ ) for  $\mathcal{L} = 20.3 \text{ fb}^{-1}$  at 8 TeV [4]. Corresponding to jet multiplicities from two to six, they introduced five inclusive analyses channels labelled as A to E (for the details of the cuts see Table 1 of [4]). Each channel is further divided as ‘Tight’, ‘Medium’ and ‘Loose’ depending on the final cuts on the observables  $\cancel{E}_T / m_{eff}$  and  $m_{eff}(\text{incl.})$ <sup>14</sup>. The constraints are presented in terms of an upper limit on the effective cross-section  $\sigma_{BSM}/\text{fb}$  or the number of events from BSM physics ( $N_{BSM}$ ) for each of the 10 signal regions. We use these model independent limits to derive new limits on  $m_{\tilde{g}}$  in this section. The observed upper limits on  $N_{BSM}$  at 95 % Confidence Level (CL) for signal regions SRA-Light, SRA-Medium, SRB-Medium, SRB-Tight, SRC-Medium, SRC-Tight, SRD, SRC-Loose, SRE-Tight, SRE-Medium, SRE-Loose are 1341, 51.3, 14.9, 6.7, 81.2, 2.4, 15.5, 92.4, 28.6, 8.3 respectively [4].

For single lepton ( $n = 1$ ) analysis we use the “hard single-lepton channel” introduced in [5]. Selection criteria for the signal regions are listed in Table 4 of Ref. [5]. For each jet multiplicity ATLAS collaboration defined two sets of requirements - an inclusive signal region and a binned one. In the absence of signal events they put upper limits on  $N_{BSM}$  at 95 % CL with  $\mathcal{L} = 20.3 \text{ fb}^{-1}$  for 6 signal regions (see Table 17 of Ref. [5]). Furthermore, in this analysis the electron and the muon channels are treated independently. For the binned hard single-lepton channels 3-jet (electron), 3-jet (muon), 5-jet (electron), 5-jet (muon), 6-jet (electron), 5-jet (muon) the upper limits on number of events are 19.8, 11.6, 12.7, 7.7, 6.6, 7.1 respectively. For inclusive hard single-lepton channels 3-jet (electron), 3-jet (muon), 5-jet (electron), 5-jet (muon), 6-jet (electron), 5-jet (muon) the upper limits on the number of events are 6.0, 7.7, 6.0, 4.6, 4.6, 3.0 respectively.

---

<sup>14</sup> $m_{eff}$  is defined as the scalar sum of the transverse momenta of the leading N jets which defines the signal region and  $\cancel{E}_T$ .  $m_{eff}(\text{incl.})$  is defined as the scalar sum of the transverse momenta of the jets having  $P_T$  greater than 40 GeV and  $\cancel{E}_T$ .

For the  $n = 2$  (SSD) analysis, ATLAS group defined three signal regions (SR0b, SR1b, SR3b) depending on the number of tagged b jets [6]. Since we consider all three generations of squarks, including  $\tilde{t}_1$  to be heavier than the gluino and mass degenerate, here the signal events are mainly sensitive to the 0b tagged data. Details of the selection cuts are discussed in Table 1 of [6]. Analysing  $20.7 \text{ fb}^{-1}$  data recorded during LHC 8 TeV run, ATLAS collaboration obtained the upper limits on the number of signal events in SR0b, SR1b and SR3b are 6.7, 11.0 and 7.0 respectively at 95 % CL.

We adopt the different selection criteria for varying signal regions discussed above. For b-tagging we use the  $P_T$  dependent b-tagging efficiency obtained by ATLAS collaboration [81]. We check that our efficiencies for different cuts used in various signal regions match with what ATLAS obtained for some benchmark points in Refs. [4–6].

Points	Limit on $m_{\tilde{g}}$ (GeV)		
	$jets + 0l + \cancel{E}_T$ [4]	$jets + 1l + \cancel{E}_T$ [5]	$jets + 2l + \cancel{E}_T$ [6]
BP1	950	1125	885
BP2	860	1140	950
BP3	1015	1110	810
BP4	1150	1175	-
BP5	750	1155	945
BP6	1015	1140	875
BP7	1105	1080	-
BP8	1110	1025	-
BP9	1250	1010	-
BP10	1240	1010	-

Table 3: Limits on  $m_{\tilde{g}}$  using the ATLAS  $jets + 0l + \cancel{E}_T$  data [4],  $jets + 1l + \cancel{E}_T$  data [5] and the  $jets + 2l + \cancel{E}_T$  (SSD) data [6].

Next we compute the number of events in different channels from gluino pair production for a given  $m_{\tilde{g}}$  for different benchmark points in Table 1. For signal event generation we use PYTHIA (v6.428) [43] and the NLO cross-section for the  $\tilde{g}\tilde{g}$  pair production is computed by PROSPINO

2.1 [71] with CTEQ6.6M PDF [72]. Comparing the computed number with the corresponding upper limits on  $N_{BSM}$  in the relevant SRs and adjusting  $m_{\tilde{g}}$  accordingly, we derive the new limits on  $m_{\tilde{g}}$  in  $0l, 1l, 2l$  (SSD) channels. The results are presented in Table 3.

It may be noted that in most cases the strongest limit on  $m_{\tilde{g}}$  comes from the hard single lepton ( $1l$ ) data [5]. This limit varies from 1010 to 1175 GeV. The results are in the same ball park as the limits obtained by ATLAS for heavy squarks in mSUGRA and in many simplified models [5].

As has already been discussed, most of the scenarios considered by us lead to leptonically enriched final states. However, leptons are soft in many cases due to small energy release in the concerned decay processes. As a result although the  $1l$  signal is strong, the dilepton signal is rather weak in such cases. Moreover, the presence of at least one hard lepton in most events tends to weaken the bound from the  $n = 0$  channel. In fact a comparison of the  $m_{\tilde{g}}$  limits in the  $n = 0$  and  $n = 2$  (SSD) channels in different scenarios suggests a suitable strategy for discriminating among them as we will see below.

In BP9 and BP10  $\tilde{\chi}_1^\pm$  is much heavier than the LSP. As a result, for relatively light gluinos, the gluino decays dominantly into the  $\bar{q}q\tilde{\chi}_1^0$  channel. This suppresses the  $1l$  events and practically depletes the dilepton signal in spite of the fact that  $\tilde{\chi}_1^\pm$  and  $\tilde{\chi}_2^0$  decay copiously into  $e$  and  $\mu$ . The strongest limits come from the  $n = 0$  channel for BP9 and BP10. The same effect is seen for BP4 albeit to a lesser extent. Here the limits from the  $n = 0$  and  $n = 1$  channels are comparable.

Depletion of the SSD channel is also seen for BP7 and BP8. In the former case BR of chargino decay to  $q\bar{q}\tilde{\chi}_1^0$  is 66%. In the latter case with a heavy L-slepton, the suppression is due to the fact that  $\tilde{\chi}_1^\pm$  and  $\tilde{\chi}_2^0$  decay mainly into  $\tau$  rich final states with almost 100% BR. In contrast to BP2 and BP5 the mass difference between  $\tilde{\chi}_1^\pm$  and the L-slepton as well as that between L-slepton and the LSP is relatively large. Thus the  $n = 2$  (SSD) channel yields stronger limits than that for  $n = 0$ .

It is worth noting from Table 3 that irrespective of the EW sector considered in Sec. 3,  $m_{\tilde{g}}$  limit is unlikely to be way below 1.1 TeV when limits from all channels are taken into account.

We next consider the three ratios  $r_1, r_2$  and  $r_3$  with relatively small theoretical errors introduced at the beginning of this section and defined in Table 4. This table is computed for  $m_{\tilde{g}} = 1.25$  TeV which is just beyond the reach of recently concluded LHC experiments (see Table 3). Of course all three ratios are not independent. But their associated errors though expected to be small, may be

Points	$r_1 = \frac{S(0l+j+\cancel{E}_T)}{S(1l+j+\cancel{E}_T)}$	$r_2 = \frac{S(0l+j+\cancel{E}_T)}{S(2l+j+\cancel{E}_T)}$	$r_3 = \frac{S(1l+j+\cancel{E}_T)}{S(2l+j+\cancel{E}_T)}$
BP1	1.85	13.16	7.12
BP2	1.35	6.30	4.67
BP3	2.42	24.10	9.94
BP4	1.45	8.31	5.75
BP5	1.17	4.48	3.84
BP6	1.91	19.04	9.98
BP7	4.16	215.91	51.96
BP8	4.88	287.36	58.91
BP9	1.70	11.29	6.64
BP10	3.06	34.02	11.10

Table 4: Here  $r_1$  (  $r_2$  ) represents the ratio of number of events from SRD 0l signal region [4] with “Inclusive-5j1 $\mu$ ” single lepton signal [5](“SR0b” SSD signal [6]) region for  $m_{\tilde{g}} = 1.25$  TeV.

different in each case. We quote the results for all three with the hope that the two having the least errors may settle the issue once sufficient data is accumulated. It follows from Table 4 that if one of the ratios for two benchmark points appears to be similar, the others will discriminate between the two. The correlation between the size of the ratios and the corresponding gluino mass limits may easily be noted.

## 6 Conclusion

The LHC searches during the 7/8 TeV runs in the  $m$ -jets +  $n$ -leptons +  $\cancel{E}_T$  channels, where  $m \geq 2$ , have obtained important limits on the masses of the strongly interacting sparticles - the squarks and the gluinos (see Refs. [4–8]). These limits, however, provide little information on the EW sparticles unless very specific SUSY breaking mechanisms like mSUGRA [25] are invoked to relate masses of the strong and EW sparticles.

The purpose of this paper is to investigate the EW sector of pMSSM [31]. In order to achieve our goal we focus on the bounds from ATLAS and CMS searches for the direct production of



$\tilde{\chi}_1^\pm \tilde{\chi}_2^0$  [15, 17] and slepton pairs [16, 17] via the hadronically quiet channels with large  $\cancel{E}_T$ . We also include in our analysis the WMAP/PLANCK constraints [19, 20] on the observed DM relic density and require  $a_\mu^{\text{SUSY}}$  to agree with  $\Delta a_\mu$  at the level of  $2\sigma$  (Sec. 2) [18]. The observables under consideration while sensitive to the EW sectors of SUSY models, are by and large independent of the strongly interacting sparticles. Moreover, the measurement of  $m_h$  enables us to study LSP pair annihilation into the h-resonance more precisely.

The main conclusion of this paper is that for a fairly large number of pMSSM models [31] without specific assumptions for soft SUSY breaking, the EW sectors are constrained by the above data (see Figs.1 - 10). In many cases the constraints are quite severe while they are a little relaxed in the other cases. However, in all cases the allowed parameter space (APS) is a bounded region indicating both upper and lower bounds on EW sparticle masses.

Using the model independent limits on  $N_{BSM}$  (defined in Sec. 3.1) as obtained by ATLAS and CMS, we constrain the EW sectors of several pMSSM models closely related to the simplified models considered by the LHC collaborations. The models are characterized by different mass hierarchies among the EW sparticles. The simplified models showcase the basic features of dedicated LHC searches but it is important to relate the search results with indirect observables like the DM relic density and  $(g-2)_\mu$ . They also involve unrealistic assumptions like  $M_{\tilde{L}} = M_{\tilde{E}}$  (see Sec. 3.1) and consequently miss some phenomenologically interesting possibilities like the invisible decays of  $\tilde{\chi}_2^0$  with  $\approx 100\%$  BR (see Sec. 3.1.1). We have used the ATLAS and CMS data to derive new constraints in several models which are interesting in their own right but not included in Refs. [15–17].

We focus on models with bino dominated LSP, wino dominated  $\tilde{\chi}_1^\pm$  and  $\tilde{\chi}_2^0$  along with light sleptons. All strongly interacting sparticles and the heavier Higgs bosons are assumed to be decoupled. These models are highly sensitive to the trilepton signal from  $\tilde{\chi}_1^\pm \tilde{\chi}_2^0$  pair production. In this analysis we have also taken into account the limits from direct slepton searches (Sec.3.5 and Sec.3.6) which sometimes cover parameter spaces insensitive to the trilepton data.

We now summarize the results for the models with relatively light  $\tilde{\chi}_1^\pm$  and  $\tilde{\chi}_2^0$  and sleptons (L-type or R-type or both) lighter than the above gauginos (Figs.1 - 7). The tilted LGLS- $\tilde{\chi}_1^0$  model (Sec. 3.1.1, Fig.2(a)), for low values of  $\tan\beta$ , is disfavoured by the combined constraints. The LGLRS- $\tilde{\chi}_1^0$  model (Sec. 3.2.1 Figs.5(a), 5(b)) for both low and high  $\tan\beta$  is also not viable. The last two constraints follow from both chargino-neutralino and direct slepton searches and illustrate

the interplay between different search channels. All the other models in this category have APS consistent with combined constraints.

Within pMSSM a few DM producing mechanisms are possible which are not viable in specific models like mSUGRA [30]. LSP-sneutrino coannihilation is a case in point. However, the combined constraints used in our analysis put severe restrictions on some of the pMSSM allowed mechanisms. Bulk annihilation, for example, is disfavoured as the dominant relic density producing mechanism in all models except for one (see Fig.10(a)). Only in the LLRS model with small  $\tan\beta$  the tip of the near vertical red dotted region representing bulk annihilation is consistent with all constraints. The LSP pair annihilation into a light Higgs resonance can produce the required DM relic density for low  $\tan\beta$  only. But the LHC constraints rule this out for low  $m_{\tilde{\chi}_1^\pm}$ . As a result the SUSY contribution to  $(g-2)_\mu$  is suppressed leading to a tension with the measured value. Only if the  $(g-2)_\mu$  constraint is relaxed to the level of  $3\sigma$ , this option is viable in a few cases (see Figs.4(a), 5(a), 10(a))<sup>15</sup>. For similar reasons LSP annihilation into the Z-resonance is also not viable. Thus, in contrast to the LSP pair annihilation, various coannihilation processes survive as the main DM producing mechanisms favoured in most scenarios over large regions of parameter space.

It is well known that the coannihilation mechanisms operate on narrow strips in each parameter space. The combination of theoretical constraints/ LEP limits, the LHC exclusion contours and the  $(g-2)_\mu$  constraint at the level of  $2\sigma$  restrict the lower and the upper edges of this strip. Thus in each of the APS under consideration the EW sparticles have their masses bounded from both above and below.

We have also analysed models with heavy sleptons and lighter  $\tilde{\chi}_1^\pm, \tilde{\chi}_2^0$  (Sec. 3.4 and Fig.8). In this case the LHC constraints are relatively weak. Nevertheless the strip allowed by WMAP/PLANCK data arising from LSP -  $\tilde{\chi}_1^\pm / \tilde{\chi}_2^0$  coannihilation is bounded by the  $(g-2)_\mu$  constraint at the level of  $2\sigma$ .

Models with light sleptons and heavy as well as decoupled  $\tilde{\chi}_1^\pm, \tilde{\chi}_2^0$  have also been considered in this analysis. We have analysed the LLS (Sec. 3.5, Fig.9) and the LLRS (Sec. 3.6 and Fig.10) models with high and low  $\tan\beta$ . In all cases  $m_{\tilde{\chi}_1^\pm}$  is assumed to be beyond the direct LHC search limit. We find a bounded APS in each case. For the LLS model LSP-sneutrino coannihilation is

---

<sup>15</sup>It may be recalled that in the LGHS model (see Sec. 3.4) the Higgs resonance mechanism can not be excluded beyond doubt since the spoiler mode may weaken the trilepton signal.

responsible for the right amount of relic density. In the LLRS model  $\mu$  has to be large to ensure a wino dominated chargino. As a result for both choices of  $\tan\beta$  we find  $\tilde{\tau}_1$  to be the NLSP and LSP undergoes coannihilation with it to produce the required amount of DM relic density. For low  $\tan\beta$ , LSP pair annihilation into the h-resonance is also viable for slepton masses beyond the LHC reach. This possibility, however, is in conflict with the  $(g-2)_\mu$  constraint at the  $2\sigma$  level. We note in passing that the light right slepton (LRS) model is inconsistent with the  $(g-2)_\mu$  limit.

We have also studied the impact of the direct and indirect searches of DM on the APS of different models after filtering them through the above three constraints. We would however like to remind the readers of the inherent theoretical, experimental and astrophysical uncertainties and ambiguities involved in the analysis as reviewed in details in the text (see Sec.1 and Sec.2.3).

After including the DM direct detection limits, it follows from Fig.11(a) that there is a tension between two models and the XENON100 [21]/ LUX [22] data. These are the LGLS model (Fig.1(a)) and the tilted LGLS- $\tilde{\chi}_1^\pm$  model (Fig.3(a)) at low  $\tan\beta$ . Modulo the aforesaid uncertainties the LGLRS (Fig.4(a)) and the tilted LGLRS- $\tilde{\chi}_1^\pm$  (Fig.6(a)) scenarios at low  $\tan\beta$  are also in conflict with the direct detection data (Fig.11(b)). The XENON1T experiment [23] is expected to scrutinize all the remaining models closely.

It follows from Fig.12 that the other cases namely the LGRS, LGHS, LLS and LLRS models (see Fig.7 to Fig.10) are fairly insensitive to XENON100 [21] and LUX [22] data. XENON1T [23] can spell the final verdict on the LGHS and LGRS models. The remaining models will be probed by the XENON1T [23] if the theoretical and astrophysical uncertainties are brought under control.

Next we consider the possible impacts of the above scenarios on the next round of experiments at LHC. However, it will be hard to establish the underlying model and the DM producing mechanism in the early stages of the experiment even if SUSY is discovered. Therefore we explore the possibility of identifying the observables which are sensitive to different DM producing mechanisms. This may be possible if at least one of the strongly interacting sparticles are relatively light. The feasibility of this approach has already been demonstrated by considering the light stop, the light stop-gluino and the light gluino scenarios and observables based on the  $n$ -leptons +  $m$ -jets +  $\cancel{E}_T$  signal for different values of  $n$  [30, 40].

In this paper we focus on the light gluino scenario (see Sec. 5). We choose characteristic benchmark points from Figs.1 to 10 (excluding Figs.2(a), 5(a) and 5(b)) which are allowed by the

combined constraints and correspond to different relic density producing mechanisms (see Tables 1 and 2). Using the latest ATLAS data in search channels with  $n = 0$  [4],  $n = 1$  [5] and  $n = 2$  (same sign dilepton) [6], we reanalyse the gluino mass limits in all cases (see Table 3). In our generator level simulation we have adopted the selection criteria of Refs. [4–6].

It is worth noting that the  $m_{\tilde{g}}$  limit varies considerably with the search channel for each BP. For different scenarios the strongest limit comes from channels corresponding to different  $n$ . For all scenarios with a L-slepton lighter than the  $\tilde{\chi}_1^\pm$  (BP 1-6), these limits come from the  $n = 1$  channel. In the remaining cases (BP 7 - 10) the  $n = 0$  channel yields the best limits. However, the above limits for all scenarios lie in a reasonably narrow range: 1105 - 1250 GeV. Thus the limit on  $m_{\tilde{g}}$  is only moderately sensitive to the EW sector if it is derived from a multichannel analysis.

Taking cue from the above discussion the observables which may potentially discriminate among various scenarios can be introduced. We define three ratios  $r_1$ ,  $r_2$  and  $r_3$  (Table 4) that are associated with relatively small theoretical errors (see Sec. 5). They are derived using the event rates for  $n = 0$ , 1 and 2 for a gluino mass of 1.25 TeV which is just beyond the reach of the recently concluded LHC experiments (see Table 3). The values of these ratios indeed illustrate that sufficiently accurate measurements may discriminate among the underlying scenarios.

**Acknowledgments :** AD acknowledges the award of a Senior Scientist position by the Indian National Science Academy. MC would like to thank Council of Scientific and Industrial Research, Government of India for financial support.

## References

- [1] For reviews on supersymmetry, see, *e.g.*, H. P. Nilles, Phys. Rep. **110**, 1 (1984); J. D. Lykken, [arXiv:hep-th/9612114]; J. Wess and J. Bagger, *Supersymmetry and Supergravity*, 2nd ed., (Princeton, 1991).
- [2] H. E. Haber and G. Kane, Phys. Rep. **117**, 75 (1985); S. P. Martin, [arXiv:hep-ph/9709356]; D. J. H. Chung *et al.*, Phys. Rept. **407**, 1 (2005) [arXiv:hep-ph/0312378].
- [3] M. Drees, P. Roy and R. M. Godbole, *Theory and Phenomenology of Sparticles*, (World Scientific, Singapore, 2005); H. Baer and X. Tata, *Weak scale supersymmetry: From superfields to scattering events*, Cambridge, UK: Univ. Pr. (2006) 537 p.

- [4] ATLAS Collaboration, ATLAS-CONF-2013-047 [<http://cds.cern.ch/record/1547563>].
- [5] ATLAS Collaboration, ATLAS-CONF-2013-062 [<http://cds.cern.ch/record/1557779>].
- [6] ATLAS Collaboration, ATLAS-CONF-2013-007 [<https://cds.cern.ch/record/1522430>].
- [7] ATLAS Collaboration, JHEP **10** (2013) 130 [arXiv:1308.1841]; ATLAS Collaboration, ATLAS-CONF-2013-061 [<https://cds.cern.ch/record/1557778>]; ATLAS Collaboration, ATLAS-CONF-2013-026 [<https://cds.cern.ch/record/1525882>].
- [8] CMS Collaboration, Eur. Phys. J. C **73**, 2568 (2013) [arXiv:1303.2985]; CMS PAS SUS-13-004, [<https://cds.cern.ch/record/1596446>].
- [9] T. J. LeCompte and S. P. Martin, Phys. Rev. D **85**, 035023 (2012) [arXiv:1111.6897]. H. K. Dreiner, M. Kramer and J. Tattersall, Europhys. Lett. **99** (2012) 61001 [arXiv:1207.1613]; B. Bhattacharjee and K. Ghosh, [arXiv:1207.6289]; B. Bhattacharjee, A. Choudhury, K. Ghosh and S. Poddar, Phys. Rev. D **89**, 037702 (2014) [arXiv:1308.1526]; T. Cohen *et al.*, [arXiv:1311.6480]; S. Mukhopadhyay, M. M. Nojiri and T. T. Yanagida, [arXiv:1403.6028]; M. Low and L. T. Wang, [arXiv:1404.0682].
- [10] N. Sakai, Zeit. Phys. C **11** (1981) 153; R. K. Kaul and P. Majumdar, Nucl. Phys. B **199** (1982) 36; R. Barbieri and G. F. Giudice, Nucl. Phys. B **306** (1988) 63.
- [11] K. L. Chan, U. Chattopadhyay and P. Nath, Phys. Rev. D **58**, 096004 (1998); [arXiv:hep-ph/9710473]; J. L. Feng, K. T. Matchev and T. Moroi, Phys. Rev. D **61**, 075005 (2000); Phys. Rev. Lett. **84**, 2322 (2000) [arXiv:hep-ph/9908309]; U. Chattopadhyay, A. Corsetti and P. Nath, Phys. Rev. D **68**, 035005 (2003) [arXiv:hep-ph/0303201]; S. Akula, M. Liu, P. Nath and G. Peim, Phys. Lett. B **709**, 192 (2012) [arXiv:1111.4589] J. L. Feng, Ann. Rev. Nucl. Part. Sci. **63** (2013) 351-382, [arXiv:1302.6587]; H. Baer, V. Barger, M. Padeffke-Kirkland and X. Tata, Phys. Rev. D **89** (2014) 037701, [arXiv:1311.4587]; H. Baer, V. Barger, D. Mickelson and M. Padeffke-Kirkland, [arXiv:1404.2277]; A. Mustafayev and X. Tata, [arXiv:1404.1386].
- [12] The LEP SUSY Working Group, [<http://lepsusy.web.cern.ch/lepsusy/>].
- [13] CDF collaboration, T. Aaltonen *et al.*, [CDF public note 10636 (2011)].

- [14] DØ Collaboration, V. Abazov *et al.*, Phys. Lett. B **680** (2009) 34 [arXiv:0901.0646].
- [15] ATLAS Collaboration, ATLAS-CONF-2013-035 [https://cds.cern.ch/record/1532426].
- [16] ATLAS Collaboration, ATLAS-CONF-2013-049 [https://cds.cern.ch/record/1547565].
- [17] CMS Collaboration, CMS PAS SUS-13-006 [https://cds.cern.ch/record/1563142].
- [18] Muon G-2 Collaboration, Phys. Rev. D **73** (2006) 072003 [arXiv:hep-ex/0602035]; B. L. Roberts, Chin. Phys. C **34** (2010) 741744 [arXiv:1001.2898].
- [19] G. Hinshaw *et al.*, (WMAP Collaboration), [arXiv:1212.5226].
- [20] P. A. R. Ade, *et al.*, [Planck Collaboration], [arXiv:1303.5076].
- [21] XENON100 Collaboration, E. Aprile *et al.*, Phys. Rev. Lett. **109**, 181301 (2012) [arXiv:1207.5988].
- [22] LUX Collaboration, D. S. Akerib *et al.*, arXiv:1310.8214.
- [23] XENON1T Collaboration, E. Aprile *et al.*, Phys. Rev. Lett. **109**, 181301 (2012) [arXiv:1206.6288].
- [24] M. Ackermann *et al.* [Fermi-LAT Collaboration], Phys. Rev. Lett. **107** (2011) 241302 [arXiv:1108.3546].
- [25] A. H. Chamseddine, R. Arnowitt and P. Nath, Phys. Rev. Lett. **49**, 970 (1982); R. Barbieri, S. Ferrara and C. A. Savoy, Phys. Lett. B **119** (1982) 343; L. J. Hall, J. Lykken and S. Weinberg, Phys. Rev. D **27**, 2359 (1983); P. Nath, R. Arnowitt and A. H. Chamseddine, Nucl. Phys. B **227**, 121 (1983); N. Ohta, Prog. Theor. Phys. **70**, 542 (1983).
- [26] C. Jungman, M. Kamionkowski and K. Griest, Phys. Rep. **267**, 195 (1996) [arXiv:hep-ph/9506380]; G. Bertone, D. Hooper and J. Silk, Phys. Rept. **405**, 279 (2005) [arXiv:hep-ph/0404175];
- [27] A. Lahanas, N. Mavromatos and D. Nanopoulos, Int. J. Mod. Phys. D **12**, 1529 (2003) [arXiv:hep-ph/0308251]; W. L. Freedman and M. S. Turner, Rev. Mod. Phys. **75**, 1433 (2003) [arXiv:astro-ph/0308418]; L. Roszkowski, Pramana **62**, 389 (2004) [arXiv:hep-ph/0404052];

- K. Olive, [arXiv:astro-ph/0503065]; H. Baer and X. Tata, [arXiv:0805.1905], in *Physics at the Large Hadron Collider*, Indian National Science Academy, A Platinum Jubilee Special Issue (Eds. A. Datta, B. Mukhopadhyaya and A. Raychaudhuri; Springer, 2009). M. Drees, [arXiv:1204.2373]; S. Arrenberg *et al.*, [arXiv:1310.8621].
- [28] G. Belanger, F. Boudjema, A. Cottrant, R. M. Godbole and A. Semenov, Phys. Lett. B **519**, 93 (2001) [arXiv:hep-ph/0106275]; U. Chattopadhyay, D. Das, P. Konar and D. P. Roy, Phys. Rev. D **75**, 073014 (2007) [arXiv:hep-ph/0610077]; U. Chattopadhyay, D. Das, A. Datta and S. Poddar, Phys. Rev. D **76**, 055008 (2007) [arXiv:0705.0921]; R. M. Godbole, M. Guchait and D. P. Roy, Phys. Rev. D **79**, 095015 (2009) [arXiv:0807.2390]; U. Chattopadhyay and D. Das, Phys. Rev. D **79**, 035007 (2009) [arXiv:0809.4065]; U. Chattopadhyay, D. Das and D. P. Roy, Phys. Rev. D **79**, 095013 (2009) [arXiv:0902.4568]; D. Feldman, Z. Liu and P. Nath, Phys. Rev. D **80**, 015007 (2009) [arXiv:0905.1148]; D. Feldman, Z. Liu, P. Nath and B. D. Nelson, Phys. Rev. D **80**, 075001 (2009) [arXiv:0907.5392]; U. Chattopadhyay, D. Das, D. K. Ghosh and M. Maity, Phys. Rev. D **82**, 075013 (2010) [arXiv:1006.3045]; M. A. Ajaib, T. Li and Q. Shafi, Phys. Rev. D **85**, 055021 (2012) [arXiv:1111.4467]; A. Choudhury and A. Datta, Mod. Phys. Lett. A **27** (2012) 1250188 [arXiv:1207.1846]; S. Mohanty, S. Rao and D. P. Roy, J. High Energy Phys. **11** (2012) 175 [arXiv:1208.0894]; S. Bhattacharya, S. Chakdar, K. Ghosh and S. Nandi, Phys. Rev. D **89**, 015004 (2014), [arXiv:1309.0036]; K. Harigaya, K. Kaneta and S. Matsumoto, [arXiv:1403.0715].
- [29] D. A. Vasquez, G. Belanger and C. Boehm, Phys. Rev. D **84**, 095015 (2011) [arXiv:1108.1338]; A. J. Williams, C. Boehm, S. M. West and D. A. Vasquez, Phys. Rev. D **86**, 055018 (2012) [arXiv:1204.3727]; A. Arbey, M. Battaglia, A. Djouadi, F. Mahmoudi, Phys. Lett. B **720** (2013) 153, [arXiv:1211.4004]; G. Arcadi, R. Catena and P. Ullio, [arXiv:1211.5129]; C. Boehm, P. S. B. Dev, A. Mazumdar and E. Pukartas, JHEP **06** (2013) 113 [arXiv:1303.5386]; S. Scopel, N. Fornengo and A. Bottino, [arXiv:1304.5353]; J. A. Casas, J. M. Moreno, K. Rolbiecki and B. Zaldivar, [arXiv:1305.3274]; B. Bhattacharjee, M. Chakraborti, A. Chakraborty, U. Chattopadhyay, D. Das and D. K. Ghosh, Phys. Rev. D **88** (2013) 035011 [arXiv:1305.4020] A. Fowlie *et al.*, Phys. Rev. D **88**, 055012 (2013) [arXiv:1306.1567]; A. Arbey, M. Battaglia and F. Mahmoudi, Phys. Rev. D **88**, 095001 (2013) [arXiv:1308.2153]; A. Pierce, N. R. Shah, K.



Freese [arXiv:1309.7351].

- [30] A. Choudhury and A. Datta, JHEP **06** (2012) 006 [arXiv:1203.4106].
- [31] A. Djouadi *et al.* [MSSM Working Group Collaboration], [hep-ph/9901246].
- [32] S. Akula, D. Feldman, Z. Liu, P. Nath and G. Peim, Mod. Phys. Lett. A **26** (2011) 1521 [arXiv:1103.5061]; N. Bhattacharyya, A. Choudhury and A. Datta, Phys. Rev. D **83**, 115025 (2011) [arXiv:1104.0333]; N. Bhattacharyya, A. Choudhury and A. Datta, Phys. Rev. D **84**, 095006 (2011) [arXiv:1107.1997]; S. Akula *et al.*, Phys. Rev. D **85**, 075001 (2012) [arXiv:1112.3645]; K. A. Olive, [arXiv:1202.2324]; D. Ghosh, M. Guchait, S. Raychaudhuri and D. Sengupta, Phys. Rev. D **86**, 055007 (2012) [arXiv:1205.2283]; A. Fowlie *et al.*, Phys. Rev. D **86**, 075010 (2012) [arXiv:1206.0264]; M. Cannoni, O. Panella, M. Pioppi and M. Santoni, Phys. Rev. D **86**, 037702 (2012) [arXiv:1206.5759]; P. Nath, [arXiv:1207.5501]; O. Buchmueller *et al.*, Eur. Phys. J. C **72** (2012) 2243 [arXiv:1207.7315]; M. Chakraborti, U. Chattopadhyay and R. M. Godbole, Phys. Rev. D **87**, 035022 (2013) [arXiv:1211.1549].
- [33] M. Citron *et al.*, Phys. Rev. D **87**, 036012 (2013), [arXiv:1212.2886]; K. Kowalska, L. Roszkowski, E. M. Sessolo, JHEP **06** (2013) 078, [arXiv:1302.5956]; S. H.-Versille *et al.*, [arXiv:1309.6958]; P. Bechtle *et al.*, [arXiv:1310.3045]; O. Buchmueller *et al.*, [arXiv:1312.5250]; J. Ellis, [arXiv:1312.5426].
- [34] V. A. Mitsou, Int. J. Mod. Phys. A **28** (2013) 1330052, [arXiv:1310.1072];  
See also: C. Arina and M. E. Cabrera, [arXiv:1311.6549]; U. Haisch, A. Hibbs and E. Re, Phys. Rev. D **89**, 034009 (2014) [arXiv:1311.7131]; G. Arcadi, Y. Mambrini, M. H. G. Tytgat and B. Zaldivar, [arXiv:1401.0221].
- [35] H. Baer, T. Krupovnickas, A. Mustafayev, E. -K. Park, S. Profumo and X. Tata, JHEP **0512** (2005) 011 [hep-ph/0511034].
- [36] ATLAS Collaboration, Phys. Lett. B **716** (2012) 1-29 [arXiv:1207.7214]; CMS Collaboration, Phys. Lett. B **716** (2012) 30-61 [arXiv:1207.7235].
- [37] ATLAS collaboration, Phys. Lett. B **718** (2013) 879 [arXiv:1208.2884].
- [38] ATLAS collaboration, Phys. Lett. B **718** (2013) 841 [arXiv:1208.3144].



- [39] CMS Collaboration, JHEP **11** (2012) 147 [arXiv:1209.6620].
- [40] A. Choudhury and A. Datta, JHEP **09** (2013) 119 [arXiv:1305.0928].
- [41] ATLAS Collaboration, ATLAS-CONF-2013-154 [https://cds.cern.ch/record/1493493].
- [42] CMS Collaboration, CMS-PAS-SUS-12-022 [http://cdsweb.cern.ch/record/1496092].
- [43] T. Sjostrand, S. Mrenna and P. Skands, JHEP **05** (2006) 026 [arXiv:hep-ph/0603175].
- [44] E. W. Kolb and M. S. Turner, “*The Early universe*, Front. Phys. 69, 1 (1990).
- [45] K. Hagiwara, R. Liao, A. D. Martin, D. Nomura and T. Teubner, J. Phys. G G38 (2011) 085003 [arXiv:1105.3149].
- [46] A. Nyffeler, arXiv:1312.4804 and references therein.
- [47] M. Davier, A. Hoecker, B. Malaescu and Z. Zhang, Eur. Phys. J. C **71**, 1515 (2011) [arXiv:1010.4180], Erratum Ibid. C72 (2012) 1874.
- [48] A. Djouadi, Phys. Rept. 459 (2008) 1 [arxiv:hep-ph/0503173].
- [49] G. Degrandi, S. Heinemeyer, W. Hollik, P. Slavich and G. Weiglein, Eur. Phys. J. C **28**, 133 (2003) [arxiv:hep-ph/0212020]; B. C. Allanach, A. Djouadi, J. L. Kneur, W. Porod and P. Slavich, JHEP **09**, 044 (2004) [arxiv:hep-ph/0406166]; S. P. Martin, Phys. Rev. D **75**, 055005 (2007) [arxiv:hep-ph/0701051]; R. V. Harlander, P. Kant, L. Mihaila and M. Steinhauser, Phys. Rev. Lett.(100,191602,2008) [arXiv:0803.0672], Erratum: Phys. Rev. Lett.(101,039901,2008); S. Heinemeyer, O. Stal and G. Weiglein, Phys. Lett. B **710**, 201 (2012) [arXiv:1112.3026]; A. Arbey, M. Battaglia, A. Djouadi and F. Mahmoudi, [arXiv:1207.1348].
- [50] ATLAS Collaboration, ATLAS-CONF-2013-093 [https://cds.cern.ch/record/1595756]; ATLAS Collaboration, arXiv:1402.7029.
- [51] D. Ghosh, M. Guchait and D. Sengupta, Eur. Phys. J. C **72**, 2141 (2012) [arXiv:1202.4937]; K. Howe and P. Saraswat, JHEP **10**, 065 (2012) [arXiv:1208.1542]; A. Arbey, M. Battaglia and F. Mahmoudi, [arXiv:1212.6865]; A. Bharucha, S. Heinemeyer and F. von der Pahlen, Eur. Phys. J. C **73**, 2629 (2013) [arXiv:1307.4237]; T. Han, S. Padhi and S. Su, Phys. Rev.

- D **88**, 115010 (2013) [arXiv:1309.5966]; A. Papaefstathiou, K. Sakurai and M. Takeuchi, [arXiv:1404.1077]; F. Yu, [arXiv:1404.2924].
- [52] F. Jegerlehner and A. Nyffeler, Phys. Rept. 477 (2009) 1-110 [arXiv:0902.3360].
- [53] D. A. Kosower, L. M. Krauss and N. Sakai, Phys. Lett. B **133**, 305 (1983); T. C. Yuan, R. Arnowitt, A. H. Chamseddine and P. Nath, Z. Phys. C **26**, 407 (1984).
- [54] J. L. Lopez, D. V. Nanopoulos and X. Wang, Phys. Rev. D **49**, 366 (1994); U. Chattopadhyay and P. Nath, Phys. Rev. D **53**, 1648 (1996) [arXiv:hep-ph/9507386].
- [55] T. Moroi, Phys. Rev. D **53**, 6565 (1996) (erratum - Phys. Rev. D **56**, 4424 (1997) [arXiv:hep-ph/9512396]; S. Heinemeyer, D. Stockinger and G. Weiglein, Nucl. Phys. B **690** (2004) 62 [arXiv:hep-ph/0312264] ; G. -C. Cho, K. Hagiwara, Y. Matsumoto and D. Nomura, JHEP **11** (2011) 068 [arXiv:1104.1769].
- [56] M. Endo, K. Hamaguchi, S. Iwamoto, T. Yoshinaga, JHEP **01** (2014) 123 [arXiv:1303.4256].
- [57] M. Endo, K. Hamaguchi, T. Kitahara, T. Yoshinaga, JHEP **11** (2013) 013 [arXiv:1309.3065].
- [58] U. Chattopadhyay and P. Nath, Phys. Rev. Lett. **86** (2001) 5854 [arXiv:hep-ph/0102157]; U. Chattopadhyay and P. Nath, Phys. Rev. D **66** (2002) 093001 [arXiv:hep-ph/0208012].
- [59] S. Akula, P. Nath and G. Peim, Phys. Lett. B **717** (2012) 188-192 [arXiv:1207.1839]; H. Baer *et al.*, Phys. Rev. D **87**, 035017 (2013) [arXiv:1210.3019].
- [60] S. Mohanty, S. Rao and D. P. Roy, JHEP **09** (2013) 027 [arXiv:1303.5830]; S. Akula and P. Nath, Phys. Rev. D **87** (2013) 115022 [arXiv:1304.5526]; N. Okada, S. Raza and Q. Shafi, arXiv:1307.0461; J. Chakraborty, S. Mohanty and S. Rao, JHEP **02** (2014) 074 [arXiv:1310.3620].
- [61] J. Kozaczuk and S. Profumo, arXiv:1308.5705.
- [62] M. Drees and M. Nojiri, Phys. Rev. D **48**, 3483 (1993) [arXiv:hep-ph/9307208].
- [63] J. Hisano, K. Nakayama and M. Yamanaka, Phys. Lett. B **684**, 246 (2010), [arXiv:0912.4701].
- [64] P. Gondolo, [arXiv:1311.6038].

- [65] J. R. Ellis, K. A. Olive and C. Savage, Phys. Rev. D **77**, 065026 (2008) [arXiv:0801.3656];  
H. Ohki *et al.*, Phys. Rev. D **78**, 054502 (2008) [arXiv:0806.4744]; J. Giedt, A. W. Thomas  
and R. D. Young, Phys. Rev. Lett. **103**, 201802 (2009) [arXiv:0907.4177]; M. Perelstein and  
B. Shakya, [arXiv:1208.0833].
- [66] G. Belanger, F. Boudjema, A. Pukhov and A. Semenov, Comput. Phys. Commun. **185** (2014)  
960 [arXiv:1305.0237].
- [67] C. Beskidt, W. de Boer, D.I. Kazakov, F. Ratnikov, JHEP **05** (2012) 094 [arXiv:1202.3366];  
C. Beskidt, W. de Boer, D. I. Kazakov and F. Ratnikov, Eur. Phys. J. C **72** (2012) 2166  
[arXiv:1207.3185].
- [68] J. Bovy and S. Tremaine, Astrophys. J. **756** (2012) 89 [arXiv:1205.4033].
- [69] M. Fairbairn, T. Douce and J. Swift, Astropart. Phys. **47** (2013) 45 [arXiv:1206.2693].
- [70] P. Bhattacharjee, S. Chaudhury, S. Kundu and S. Majumdar, Phys. Rev. D **87** (2013) 083525  
[arXiv:1210.2328].
- [71] W. Beenakker *et al.*, Nucl. Phys. B **515**, 3 (1998) [arXiv:hep-ph/9610490].
- [72] P. M. Nadolsky *et al.*, Phys. Rev. D **78**, 013004 (2008) [arXiv:0802.0007].
- [73] ATLAS collaboration, Eur. Phys. J. C **72**, 1909 (2012) [arXiv:1110.3174].
- [74] A. Datta, M. Guchhait and B. Mukhopadhyaya, Mod. Phys. Lett. A **10**, 1011 (1995).
- [75] A. Datta, A. Datta, M. Drees and D. P. Roy, Phys. Rev. D **61**, 055003 (2000)  
[arXiv:hep-ph/9907444].
- [76] G. Aarons *et al.*, [ILC Collaboration], [arXiv:0709.1893]; H. Baer *et al.*, [arXiv:1306.6352].
- [77] A. Datta, A. Datta and S. Raychaudhuri, Eur. Phys. J. C **1**, 375 (1998)  
[arXiv:hep-ph/9605432].
- [78] K. Grassie and P. N. Pandita, Phys. Rev. D **30**, 22 (1984); H.K. Dreiner, O. Kittel and U.  
Langenfeld, Phys. Rev. D **74**, 115010 (2006) [arXiv:hep-ph/0610020].

- [79] J. Hisano, S. Matsumoto, M. M. Nojiri and O. Saito, Phys. Rev. D **71**, 063528 (2005) [arXiv:hep-ph/0412403]. M. A. Amin and T. Wizansky, Phys. Rev. D **77**, 123510 (2008) [arXiv:0710.5517]. A. Chatterjee, D. Das, B. Mukhopadhyaya and S. K. Rai, [arXiv:1401.2527].
- [80] J. F. Navarro, C. S. Frenk and S. D. M. White, Astrophys. J. 490 (1997) 493-508 [arXiv:astro-ph/9611107].
- [81] ATLAS Collaboration, ATLAS-CONF-2012-043 [<https://cds.cern.ch/record/1435197>].